Published in final edited form as:
*ISPRS J Photogramm Remote Sens*. 2020 January ; 159: 364–377. doi:10.1016/j.isprsjprs.2019.11.018.

# Remote sensing algorithms for estimation of fractional vegetation cover using pure vegetation index values: A review

**Lin Gao**[a], **Xiaofei Wang**[a,b], **Brian Alan Johnson**[c], **Qingjiu Tian**[a,*], **Yu Wang**[d], **Jochem Verrelst**[e], **Xihan Mu**[f], **Xingfa Gu**[g,*]

[a]International Institute for Earth System Science, Nanjing University, Nanjing 210023, China

[b]Collaborative Innovation Center of South China Sea Studies, Nanjing University, Nanjing 210023, China

[c]Institute for Global Environmental Strategies, Hayama, Kanagawa 240-0115, Japan

[d]School of Remote Sensing and Information Engineering, Wuhan University, Wuhan 430079, China

[e]Image Processing Laboratory (IPL), Parc Científc, Universitat de València, Paterna, València 46980, Spain

[f]State Key Laboratory of Remote Sensing Science, College of Remote Sensing Science and Engineering, Faculty of Geographical Science, Beijing Normal University, Beijing 100875, China

[g]Institute of Remote Sensing and Digital Earth, Chinese Academy of Sciences, Beijing 100101, China

## Abstract

Green fractional vegetation cover ($f_c$) is an important phenotypic factor in the fields of agriculture, forestry, and ecology. Spatially explicit monitoring of $f_c$ via relative vegetation abundance (RA) algorithms, especially those based on scaled maximum/minimum vegetation index (VI) values, has been widely investigated in remote sensing research. Although many studies have explored the effectiveness of RA algorithms over the past 30 years, a literature review summarizing the corresponding theoretical background, issues, current state-of-the-art techniques, challenges, and prospects has not yet been published. The overall objective of the present study was to accomplish a comprehensive and systematic review of RA algorithms considering these factors based on the scientific papers published from January 1990 to November 2019. This review revealed that the key issues related to RA algorithms is the determination of the appropriate normalized difference vegetation index (NDVI) values of the full vegetation cover and bare soil (denoted hereafter by $NDVI_\infty$ and $NDVI_S$, respectively). The existing methods used to correct for these issues were investigated, and their advantages and disadvantages are discussed in depth. In literature

*Corresponding authors at: International Institute for Earth System Science, Nanjing University, Nanjing 210023, China. gaol081115@126.com (L. Gao), wangxiaofei_nju@163.com (X. Wang), johnson@iges.or.jp (B.A. Johnson), tianqj@nju.edu.cn (Q. Tian), wangyuchn@whu.edu.cn (Y. Wang), jochem.verrelst@uv.es (J. Verrelst), muxihan@bnu.edu.cn (X. Mu), guxingfa@radi.ac.cn (X. Gu).

**Declaration of Competing Interest**

The authors declare that they have no known competing financial interests or personal relationships that could have appeared to influence the work reported in this paper.


Europe PMC Funders Author Manuscripts

trends, we found that the number of reported studies in which RA algorithms were used has increased consistently over time, and that most authors tend to utilize the linear NDVI model, rather than other models in the RA algorithm family. We also found that RA algorithms have been utilized to analyze the images with spatial resolutions ranging from the sub-meter to kilometer, most commonly, using images of 30-m spatial resolution. Finally, current challenges and forward-looking insights in remote estimation of $f_c$ using RA algorithms are discussed to guide future research and directions.

**Keywords**

Vegetation fractional cover; Remote sensing; Normalized difference vegetation index; Review; Spectral unmixing

## 1 Introduction

Green fractional vegetation cover ($f_c$), which describes a vertical projection of the areal proportion of a landscape occupied by green vegetation (Deardorff, 1978), is an essential phenotypic factor used to characterize the spatial pattern of vegetation types. The synoptic quantification of $f_c$ plays a pivotal role in monitoring vegetation growth status and crop yields (Allen and Pereira, 2009; de la Casa et al., 2018), understanding Earth system processes (e.g., climate change, energy exchanges, and biogeochemical cycles) (Foley et al., 2000; Li et al., 2005; Wang et al., 2012; Wei et al., 2018), and elucidating relationships between human activities and the environment (e.g., deforestation, land degradation, desertification, and landscape reconstruction) (Jiang et al., 2017; Tong et al., 2016; Xin et al., 2008).

In the last few decades, by virtue of the huge volume of data obtained from remote sensors and the innovations in computing and image analysis technologies, the value of remote sensing image processing for retrieving $f_c$ over long time periods and large geographic extents (e.g., on a regional to global scale) has been proven repeatedly (Ge et al., 2018; Jing et al., 2011; Zeng et al., 2003). Methods for deriving $f_c$ based on remotely sensed data can be generally categorized into six groups (Guan et al., 2012; Jia et al., 2013): (i) relative vegetation abundance (RA) algorithms scaled by maximum and minimum vegetation index values (Gutman and Ignatov, 1997; Wittich and Hansing, 1995); (ii) spectral mixture analysis (SMA) algorithms (Roberts et al., 1998; Settle and Drake, 1993); (iii) spectral-based supervised classification algorithms (Friedl et al., 2002; Okin et al., 2013); (iv) physically-based models (e.g., multi-angle geometric-optical models) (Chopping et al., 2008; Xiao et al., 2016); (v) machine learning algorithms (Stojanova et al., 2010; Verrelst et al., 2012); and (vi) other approaches.

Among these methods, RA algorithms provide the simplest $f_c$-estimation approach (Mu et al., 2018) and include the following types: the semi-empirical NDVI model (Choudhury et al., 1994), linear NDVI model (Qi et al., 2000), NDVI mixture model (Wittich, 1997), and quadratic NDVI model (Carlson and Ripley, 1997), as well as analogous versions of linear and quadratic models based on vegetation indices apart from NDVI (Cho et al., 2014; Johnson et al., 2012). RA algorithms were first proposed in the 1990s to characterize




Europe PMC Funders Author Manuscripts

land surface interactions remotely (Choudhury et al., 1994; Gillies et al., 1997; Price, 1990;Valor and Caselles, 1996). Gutman and Ignatov (1998) were the first to attempt to identify the relationship between the satellite-derived scaled NDVI (*NDVI*, defined as again normalized NDVI) and $f_c$ over the global scale. Since then, because of their convenience and ease of interpretation, RA algorithms have received considerable attention in macroscopic monitoring of regional and global $f_c$, and associated land surface parameters, such as the leaf area index (LAI); impervious surface (IS) cover; soil moisture content (M); land surface emissivity (LSE); surface radiant temperature ($T_s$); evapotranspiration (ET); and surface energy fluxes (SEF). The results of literature searches in the Web of Science Core Collection database indicate that a large amount of the related literature has documented the performance of RA algorithms for specific study areas/data sources/applications since the 1990s, with approximately 35% of the relevant studies on $f_c$ using RA algorithms (see Section4). Nonetheless, throughout the history of its development, this topic has rarely been reviewed systematically. Given the increased demand for understanding the effects of environmental changes (e.g. land-use change and climate change) on the vegetation cover at regional to global scales and the growing number of publications related to RA algorithms in recent years, a systematic review of the background, issues, current status, challenges, and perspectives of RA algorithms is undoubtedly required.

The purpose of the present review is to provide a comprehensive overview of the scientific literature related to RA algorithms, to discuss the key issues identified therein, to offer possible prospects and insights for further research and directions. The specific objectives of this review are fourfold:

- **(1)** To elucidate the basic theory, assumptions, and issues related to the use of RA algorithms (Section 2);
- **(2)** To discuss the published approaches for addressing the identified issues (Section 3);
- **(3)** To review the status quo and trends in development of RA algorithms and evaluate the advantages and disadvantages of different RA algorithms by investigating the selected literature (Section 4);
- **(4)** To identify key issues that need to be considered further and priorities for the future research (Section 5).

To focus on these goals, we divided the selected literature on RA algorithms into two groups (Fig. 1): methodological issues and indirect applications. Methodological issues include the methodological origin and improvement of RA algorithms and the application of RA algorithms in the field of estimating $f_c$ based on remotely derived data. Indirect applications are those in which $f_c$ estimates are used as an intermediate variable for the derivation of other land surface parameters.

## 2 Background and issues

RA algorithms are a set of linear or non-linear functional relationships between a scaled VI (usually the NDVI) and $f_c$. They are used to estimate the green fractional vegetation cover or

Europe PMC Funders Author Manuscripts

the factional cover of photosynthetic vegetation based on the assumption that a pixel consists of a mixture of only two elements: green vegetation and soil. The theoretical basis of RA algorithms lies in the Beer–Lambert law and linear spectral mixture analysis (LSMA).

## 2.1 Semi-empirical NDVI model

A number of field observations conducted in dense, homogeneous crop canopies indicated that NDVI variations approached a saturation level asymptotically with an increase in LAI values, which could be approximately fitted to an exponential function of LAI (Asrar et al., 1984; Best and Harlan, 1985; Hatfield et al., 1984; Wiegand et al.,1990). This relationship could be expressed by the modified Beer–Lambert law as a general equation, given below, which has been validated by simulations (Baret and Guyot, 1991) and field experiments (Choudhury et al., 1994):

$$VI = VI_{\infty} + (VI_s - VI_{\infty}) \times e^{-K_{VI} \times LAI} \quad (1)$$

where $VI_{\infty}$ is the asymptotic value of the VI, when LAI tends toward infinity (usually full vegetation cover, i.e., $f_c = 1$), $VI_s$ represents the value of the vegetation index for bare soil (i.e., $f_c = 0$), and $K_{VI}$ is the extinction coefficient driven by leaf optical properties (e.g., leaf angle distribution), the direction of the sun, and the viewing angle. It is likely that $K_{VI}$ will lie in the range 0.8–1.3, when the VI is set to be NDVI for leaf inclinations between 30° and 70° (Baret and Guyot, 1991).

The fractional vegetation cover can be calculated according to:

$$f_c = 1 - P_0(0) \quad (2)$$

where $P_0(0)$ is the probability of a canopy gap fraction at 0° zenith angle, which can be described as a simple exponential function of LAI (Nilson, 1971):

$$P_0(0) = e^{-K_P \times LAI} \quad (3)$$

where $K_P$ is the attenuation factor analogous to $K_{VI}$ depending on the canopy architecture.

Hence, as a result of mathematical manipulation with Eqs. (1), (2), and (3) to eliminate LAI, the semi-empirical relationship between $f_c$ and the NDVI can be derived as follows (Baret et al., 1995; Wittich, 1997):

$$f_c = 1 - \left( \frac{NDVI - NDVI_{\infty}}{NDVI_s - NDVI_{\infty}} \right)^{K_p / K_{VI}} \quad (4)$$

According to Baret et al. (1995), the $K_p/K_{VI}$ equals to 0.6175 for the NDVI.

## 2.2 Linear NDVI model and NDVI mixture model

LSMA is the simplest and most common spectral unmixing approach. It is based on the underlying physical assumption that the amount of photon multiple scattering between

macroscopic materials is insignificant. LSMA describes a measured signal at each ground resolution element (i.e., pixel) as a linear combination of constituent spectral signatures representing the spectral characteristics of pure land-cover types (so-called endmembers) weighted according to their subpixel fractional cover (i.e. abundances) (Adams et al., 1986):

$$r = \sum_{i=1}^{n} (f_i \times r_i) + \varepsilon \tag{5}$$

where $r$ is the mixed pixel signal, $f_i$ is the fractional cover of endmember $i$, and $r_i$ is the spectral signal of endmember $i$. Here, $n$ is the total number of endmembers, and $\varepsilon$ is the model residual error term.

If only two endmembers (green vegetation and bare soil) are considered, then, following the idea of Deardorff (1978), LSMA could be directly applied to retrieve $f_c$ from the NDVI value of a mixed pixel. As a result, we can yield the highly-simplified formulation for the approximation of $f_c$ (i.e., the linear NDVI model), which is also commonly referred to as the pixel dichotomy model, dimidiate pixel model, or two-endmember model (Qi et al., 2000; Wittich and Hansing, 1995):

$$f_c = \frac{NDVI - NDVI_s}{NDVI_\infty - NDVI_s} \tag{6}$$

which can be rewritten as:

$$\begin{aligned} &f_c = a \times NDVI + b \\ &\text{with a} = \frac{1}{NDVI_\infty - NDVI_s}, \text{b} = -\frac{NDVI_S}{NDVI_\infty - NDVI_S}. \end{aligned} \tag{7}$$

The procedure described above was also further generalized into mosaic-pixel models involving variable, dense, and non-dense vegetation models by Gutman and Ignatov (1998) under the notion that the same NDVI value may be obtained from different subpixel structures with respect to vertical densities. The variable vegetation model is based on heterogeneous vegetation canopies having variable vertical densities, because more than one vegetation type may exist within a pixel, especially in a coarse resolution image. However, the extraction of information about multiple vegetation endmembers at the subpixel level based on LSMA is difficult. The latter two models (i.e., dense and non-dense vegetation) underscore homogeneous vegetation canopies with intra-class variations in vertical density. The root cause of the differences between mosaic-pixel models, however, is still an issue related to accurate derivation of the NDVI value of the vegetated part of the pixel. Therefore, in this paper, we discuss this inherent problem by only considering the linear NDVI model.

Likewise, LSMA can also be applied to the reflectance terms (i.e., red and near-infrared (NIR) bands) in the NDVI equation:

$$\rho_{i,\,pixel} = f_c \times \rho_{i,\,\infty} + (1 - f_c) \times \rho_{i,\,s} \tag{8}$$

where $\rho_{i,pixel}$, $\rho_{i,\infty}$, and $\rho_{i,s}$ are the pixel spectral reflectance, asymptotic spectral reflectance of vegetation, and bare soil spectral reflectance in the $i$ band, respectively, and $i$ is the red or NIR band. Then, by substituting the NDVI equation for Eq. (8), a non-linear relationship between NDVI and $f_c$ can be obtained (Verstraete and Pinty, 1991;Wittich, 1997):

$$f_c = \frac{NDVI - NDVI_s}{NDVI_\infty - NDVI_s + (1-a)\times(NDVI - NDVI_\infty)}, \quad \text{with } a = \frac{\rho_{r,\infty} + \rho_{NIR,\infty}}{\rho_{r,S} + \rho_{NIR,s}} \tag{9}$$

where $p_{r,\infty}$ and $p_{NIR,i}$ are the asymptotic spectral reflectance of vegetation at red and NIR wavelength, respectively. Here, $p_{r,s}$ and $p_{NIR,s}$ are the bare soil spectral reflectance at the red and NIR wavelength, respectively. For brevity, Eq. (9) is termed the NDVI mixture model. It should be noted that, although the linear NDVI model and the NDVI mixture could both be applied based on LSMA, Eqs. (6) and (9) are evidently not equivalent because of the poor performance of the NDVI in terms of the associative property (Price, 1990; Valor and Caselles, 1996). However, according to Wittich and Hansing (1995), these discrepancies between the two models are minor in the data range of $0.18 \le NDVI \le 0.69$.

## 2.3 Quadratic NDVI model

Based on experimental observations, Gillies and Carlson (1995) obtained the consistent relationship between $NDVI^\circ$ and $f_c$ (i.e., the quadratic NDVI model), which was further confirmed in another study (Carlson and Ripley, 1997). This relationship is defined as follows:

$$f_c = (NDVI^\circ)^2 = \left(\frac{NDVI - NDVI_s}{NDVI_\infty - NDVI_s}\right)^2 \tag{10}$$

Notably, the NDVI in this quadratic model is rarely substituted for other vegetation indices, as Eq. (10) is valid specifically for the NDVI.

## 2.4 Issues related to the RA algorithms

In RA algorithms, both the $NDVI_\infty$ and $NDVI_s$ parameters need to be known a priori. $NDVI_\infty$, however, is known to vary depending on the plant species and phenological cycle, while $NDVI_s$ varies by soil type. Furthermore, the NDVI is also not always an optimal VI for $f_c$ retrieval because of inherent characteristics such as its saturation problem in high density canopies and sensitivity to scale, background, and atmospheric variances.

Therefore, the major hurdle in the quantitative retrieval of $f_c$ is to develop the way how to determine the $NDVI_\infty$ and $NDVI_s$ thresholds, and how to compensate for the inherent limitations of NDVI. Furthermore, the assumption that a pixel consists only of green vegetation and bare soil ignores the non-photosynthetic vegetation (NPV), e.g., aboveground dead biomass, litter, and wood, which might introduce several uncertainties influencing $f_c$ estimates. Therefore, the way to mitigate the NPV effect is also one of the main issues affecting the inversion accuracy of RA algorithms. As the NPV effect is essentially caused

by this assumption, only the former issue has been continuously investigated in the past three decades.

## 3 Methods for correcting issues

### 3.1 Methods for determining the values of $NDVI_{\infty}$ and $NDVI_S$

The published approaches for determining the values of $NDVI_{\infty}$ and $NDVI_s$ can, in general, be divided into two categories: traditional approaches that assign a priori fixed value for the entire remotely sensed image and improved methods in which both values vary according to geographical factors, e.g., species and soil types (the reference values are listed in Table 1). The former includes:

**(1)** Identification of pure vegetation (or bare soil) pixels through field observations (e.g., global positioning system (GPS) coordinates at locations with full vegetation cover and pure bare soil (Wang and Qi, 2008) and field-measured pure vegetation/soil spectral data (Zhou et al., 2009)) or higher spatial resolution images (Imukova et al., 2015; Jiao et al., 2014);

**(2)** Direct analysis of remotely sensed images to obtain the accumulative maximum and minimum NDVI values in the area under investigation (Ge et al., 2008; Gutman and Ignatov, 1998; Wang et al.,2014);

**(3)** Application of end-member extraction approaches (e.g., pixel purity index (PPI) method and two-dimensional feature space plots) (Jia et al., 2017; Wang et al., 2014);

**(4)** Estimation of $NDVI_{\infty}$ via inversion modeling of the relationship between the remotely derived NDVI and *in situ f* measurements (Kuang et al., 2015; Xiao and Moody, 2005);

**(5)** Adoption of theoretically fixed values from the radiative transfer model (Liu et al., 2008).

However, variations in the spectral properties of vegetation (or soil) at the subpixel level are related not only to the plant species (or soil type), but also to the health of the vegetation and the leaf water content (or soil organic matter, soil moisture content, and soil surface roughness). As shown in Fig. 2, $NDVI_{\infty}$ values identified in the literature vary among different vegetation types, and significant differences are observed even within the same vegetation type. The global $NDVI_{\infty}$ values proposed by Gutman and Ignatov (1998) and Jiang et al. (2010) are generally lower than those ones obtained from a specific plant type. Similarly to $NDVI_{\infty}$, $NDVI_s$ varies over geographic regions because of changes in the chemical and physical attributes of soil, including organic matter content, grazed size, clay mineralogy, and water content from surface to undersurface even for the same scene in the image. The use of invariant $NDVI_{\infty}$ and $NDVI_s$ values is questionable, particularly for studies conducted over a large geographic area. Therefore, improved methods have been designed to compensate for these disadvantages using auxiliary data (e.g., land cover maps (Broxton et al., 2014; Vegas Galdos et al., 2012; Zeng et al., 2000; Zeng et al., 2003) and soil databases (Ding et al., 2016b; Montandon and Small, 2008; Wuet al., 2014)) or




Europe PMC Funders Author Manuscripts

data yielded by spatial interpolation techniques used in geographic information system (GIS) (Johnson et al., 2012) or multiangle observations (Mu et al., 2018; Song et al., 2017) to make both thresholds more compatible with the local vegetation/soil conditions. In the present study, we aim to bring the characteristics, advantages, and limitations of these improved methods to the attention of the remote sensing community by means of the following descriptions and in depth discussion.

**3.1.1 Evolvement of approaches to determine $NDVI_{\infty}$**—Zeng et al. (2000) developed a method to calculate the NDVI value for each land-cover category corresponding to 100% green vegetation cover (i.e., $NDVI_{c\infty}$). In their study, the annual maximum NDVI value ($NDVI_{p,max}$) for a given pixel was calculated and used as a substitute for the pixel NDVI in the numerator of Eq. (6). Furthermore, a histogram of $NDVI_{p,max}$ for each land-cover type was used to determine $NDVI_{c,\infty}$, which was used as a proxy for $NDVI_{\infty}$ in the denominator of Eq. (6). The annual maximum green vegetation fraction for a given pixel ($f_c$) was eventually quantified with a global invariant $NDVI_s$ value of 0.05, according to the following formula:

$$f_c' = \frac{NDVI_{p,max} - NDVI_s}{NDVI_{c,\infty} - NDVI_s} \tag{11}$$

Although this method has been well-documented (Miller et al., 2006; Refslund et al., 2014; Scheftic et al., 2014; Vegas Galdos et al.,2012), several issues related to its use should be discussed further. First, there is a possibility of temporal or spatial mismatch between the remotely sensed data and the published land cover products, particularly, in areas that have undergone rapid land use/land cover (LULC) changes. For example, the land cover in the South China Karst region was previously predominately shrubs and trees; however, it has been gradually converted to bare soil owing to the increased exploitation of natural resources during the last half-century. Recently, however, there has been a significant increase in the vegetation cover in large parts of this district as a result of ecological rehabilitation and conservation efforts. Therefore, if the most recent satellite images together with outdated land cover maps are used to calculate $NDVI_{c,\infty}$ in this region, the results will be unrealistic. Furthermore, the land cover product should be as accurate as possible (i.e., the LULC map should be optimized to fit the local context), or of a high resolution. Li and Zhang (2016) indicated that the $f_c'$ inversion accuracy over all of China was better with the ChinaCover product compared to the International Geosphere-Biosphere Program (IGBP) product, particularly in areas with high vegetation coverage. Second, the data for one full year from the same satellite sensor are a prerequisite for using Eq. (11) to estimate $f_c'$. Clearly, data continuity is crucial for the use of this interannual relationship described in Zeng et al. (2000). Therefore, it might not be feasible to use Eq. (11), especially in studies focused on medium to high resolution satellite remote sensing products (e.g., from the RapidEye and WorldView-2 satellites). This is due to the lack of consistency in the data availability, same as most optical remote sensing datasets. Third, $f_c'$ refers to the annual maximum green vegetation fraction. Consequently, $f_c'$ cannot be directly related to the real-time monitoring of surface greenness, although the annual maximum fractional

vegetation cover may be useful for analyzing the interannual driving relationship between spatiotemporal variations of the vegetation cover and climatic factors (e.g., precipitation and temperature). Most agronomic studies focus rather on $f_c$, which can provide real-time characterization of the vegetation growth status. In addition, the use of a fixed $NDVI_s$ value in Eq.(11) is unreasonable, in particular for large areas covered by contrasting soil types, as the soil reflectance always varies together with pedological classes.

**3.1.2 Evolvement of approaches to determine $NDVI_s$—**As opposed to conventional methods that involve setting a global invariant $NDVI_s$ value for the whole satellite image, the method proposed by Montandon and Small (2008)uses global databases of $NDVI_s$ together with information on historical $NDVI_{pixel}$ values to estimate the statistically most-likely fractional vegetation cover $(f_c^*)$:

$$f_c^* = \frac{\sum_{i=1}^{n}\left(\frac{NDVI_{pixel} - NDVI_{s,i}}{NDVI_{\infty} - NDVI_{s,i}}\right)^a}{n} \quad (12)$$

where $NDVI_{pixel}$ is the NDVI of a pixel; $NDVI_{,i}$ is the NDVI value of the *i-th* bare soil in the global soil spectral libraries and is lower than or equal to $NDVI_{pixel}$, $n$ is the number of the values meeting the condition $NDVI_{s,i} \leq NDVI_{pixel}$. $NDVI_{\infty}$ is calculated using the approach developed by Zeng et al. (2000), and $a$ is equal to 1 for the linear NDVI model and 2 for the quadratic NDVI model. It should be noted that in the case where $NDVI_{pixel}$ is greater than $NDVI_{\infty}$, the green vegetation fraction is assigned a value of 1.0.

The biases of the $NDVI_s$ estimates could lead to substantial uncertainties in the derivation of $f$ using RA algorithms (Montandon andSmall, 2008; Song et al., 2017). The use of a collection of $NDVI_{S,i}$ values at each pixel can partially mitigate the effect of uncertainties in the $NDVI_s$ estimates on the retrieval of the green vegetation fraction. However, in addition to the preceding discussion on the $NDVI_{\infty}$ calculation using the approach proposed by Zeng et al. (2000), other considerations regarding this approach should be noted. First, it is unrealistic to expect that all spectrums in the global soil spectral libraries are presented in a fine-scale study area (Johnson et al., 2012). Second, some soil spectrums in the soil spectral libraries that are not presented in the given pixel might also satisfy the criterion $NDVI_{s,i} \leq NDVI_{pixel}$. A further constraint is the use of the local historical lowest NDVI value instead of $NDVI_{pixel}$ to ascertain the range of possible $NDVI_s$ values more accurately. However, errors associated with $f_c^*$ could still occur. This is because there is no guarantee of a unique and authentic relationship between the spectrum of a soil endmember within a pixel and the soil spectral reflectance in the spectral libraries. Following the ideas of Zeng et al. (2000) and Montandon and Small (2008), Wu et al. (2014) and Ding et al. (2016b) attempted to calculate $NDVI_{\infty}$ and $NDVI_s$ for each vegetation type and soil group based on IGBP and the Harmonized World Soil Database (HWSD) classification schemes. However, the values of $NDVI_{\infty}$ and $NDVI_s$ still remain biased, as it is difficult to identify accurately the number and type of endmembers within a pixel, as well as its corresponding spectral signatures (Ding et al., 2016b; Wuet al., 2014). Third, the $f_c^*$ estimates are inherently statistical values that can be closer to the real green vegetation fraction calculated by using the NDVI values

of the authentic soil and vegetation endmembers. Fourth, in view of data interdependency, it is cumbersome to suffice the requirement of the prior knowledge of the land cover type information or the soil spectral libraries for applying the approach proposed by either Zeng et al. (2000) or Montandon and Small (2008). Hence, if no available auxiliary data exist (or these data are outdated/mismatching to the used remote sensing images), it is not clear how to use these approaches to estimate $NDVI_{\infty}$ and $NDVI_s$ values.

#### 3.1.3 Simultaneous determination of $NDVI_{\infty}$ and $NDVI_S$—

To address the invariant threshold problem discussed above, Johnson et al. (2012) attempted to use GIS spatial interpolation techniques, such as inverse distance weighting (IDW) and ordinary kriging (OK) to determine $NDVI_{\infty}$ and $NDVI_s$ at each pixel location. This approach is based on the assumption that it is likely that the spectral characteristics of the vegetation (or soil) endmember are more similar to the nearer vegetation (or soil) samples. The number of pure (vegetation or soil) samples and the performance of the spatial interpolation techniques are crucial to ensuring the accuracy of the interpolated $NDVI_{\infty}$ and $NDVI_s$ values. Consequently, this method may be more appropriate for scenarios where the multitude of pure vegetation and soil pixels are presented. However, its use might not be feasible in studies that are aimed at large geographic areas or use coarse resolution satellite images, as it is difficult to collect an adequate number of pure pixels as samples for spatial interpolation. Certainly, the use of more suitable interpolation methods can yield more reliable results.

In addition, recent studies (Mu et al., 2018; Song et al., 2017) suggested an alternative means of estimating $NDVI_{\infty}$ and $NDVI_s$ simultaneously without any prior knowledge, which usually is required in the approaches of Zeng et al. (2000) and Montandon and Small(2008). They utilized a directional reflectance dataset to develop the relationship between the directional green vegetation fraction $\left(f_c^{\theta}\right)$ and NDVI at a particular viewing zenith angle (VZA, θ) based on the linear NDVI model:

$$f_c^{\theta} = \frac{NDVI^{\theta} - NDVI_s^{\theta}}{NDVI_{\infty}^{\theta} - NDVI_s^{\theta}} \tag{13}$$

where $NDVI^{\theta}$, $NDVI_{\infty}^{\theta}$, and $NDVI_s^{\theta}$ are the directional NDVI, $NDVI_{\infty}$ and $NDVI_s$ at θ, respectively.

Using a Markov-chain model linked according to the modified Beer–Lambert law, the gap fraction for a given LAI at θ ($P_0$ (θ)) is expressed as, follows:

$$P_0(\theta) = e^{(-G(\theta)\cdot\Omega\cdot LAI)/\cos(\theta)} \tag{14}$$

where $G(\theta)$ is the projection coefficient, which is approximately 0.5 around the zenith angle of 57°, and Ω is the clumping index. Then, using the relationship defined by Eq. (2), Eqs. (13) and (14) were integrated as

$$\frac{NDVI_{\infty} - NDVI^{\theta}}{NDVI_{\infty} - NDVI_S} = e^{(-G(\theta)\cdot\Omega\cdot LAI)/\cos(\theta)} \tag{15}$$

Eq. (15) is based on the assumptions that the pure vegetation (or soil) is isotropic and that the viewing angle influences only mixed pixels consisting of vegetation and soil.

For calculating $NDVI_{\infty}$ and $NDVI_s$, in the two studies different strategies were adopted. Song et al. (2017)used the MODIS Bidirectional Reflectance Distribution Function (BRDF)/Albedo products and the Global Land Surface Satellite (GLASS) LAI product to estimate the $NDVI_{\infty}$ and $\overline{NDVI_s}$ values at the 57° VZA, using a 3 × 3 sliding window involving nine pixels and more than three equations based on Eq. (15). Mu et al. (2018) established two equations for VZAs of 55° and 60°, respectively, to describe the relationship defined by Eq.(15). Thereafter, they combined these two equations to eliminate $G$, $\Omega$, and LAI with the assumption that $G$ and Ω are invariant between VZAs of 55° and 60°:

$$\begin{aligned}&\cos 55^{\circ} \cdot \ln\left(NDVI_{\infty} - NDVI_i^{55^{\circ}}\right) - \cos 60^{\circ} \cdot \ln\left(NDVI_{\infty} - NDVI_i^{60^{\circ}}\right) \\ &= \left(\cos 55^{\circ} - \cos 60^{\circ}\right) \cdot \ln\left(NDVI_{\infty} - NDVI_s\right)\end{aligned} \tag{16}$$

where $NDVI_i^{55^{\circ}}$ and $NDVI_i^{60^{\circ}}$ are the NDVI values of pixel $i$ at VZAs of 55° and 60°, respectively. Finally, $NDVI_{\infty}$ and $\overline{NDVI_s}$ can be calculated by using Eq. (16) with nine pixels within a 3 × 3 sliding window.

Despite achieving some success, the methods proposed by Song et al. (2017) and Mu et al. (2018)still have several limitations. First, the $f_c$ estimation was conducted within a sliding window of a certain size in both studies. Consequently, the size of the sample window is important for minimizing differences in $NDVI_{\infty}$ or $\overline{NDVI_s}$ across the window pixels, as all pixels within the window have the same values of $NDVI_{\infty}$ or $\overline{NDVI_s}$. Although it was verified that a 3 × 3 window was appropriate for the 500 m or 1 km spatial resolution satellite images used in both studies, with the exception of the heterogeneity within pixel, it is still difficult to identify, whether a single vegetation type or soil group is presented in the sliding window, especially in complex and heterogeneous ecosystems. In contrast to the use of a sliding window, the time series of remotely sensed observations may be more suitable for deriving both thresholds as soil types and plant species remain unchanged for a long time in an area (Mu, personal communication). Second, these methods might be time consuming, in particular for images with large swath widths, because a number of pairs of $NDVI_{\infty}$ and $\overline{NDVI_s}$ need to be calculated within each window throughout a satellite image. Consequently, high-performance computer systems might be needed to maintain rapid computation of these methods. Third, MODIS BRDF/Albedo products were used in both studies. However, the available BRDF products obtained from spaceborne sensors are relatively limited in number and coarse in spatial resolution. In addition, it should be noted that the improved methods proposed by Zeng et al. (2000),Montandon and Small (2008), Song et al. (2017), and Mu et al. (2018)were all applied to cases where coarse spatial resolution satellite images (mostly MODIS data) were used. Considering the performance of these methods using higher spatial resolution remote sensing images (or images other than the MODIS data), their applicability still needs further validation.

### 3.2 Methods for correcting NDVI defects

The NDVI is the most commonly used index for remote sensing of vegetation. Despite its usefulness, the NDVI is known to be saturated at high LAI levels and vulnerable to atmospheric perturbations, scaling, and soil background effects. Thus, the use of other more robust vegetation indices as substitutes for the NDVI of linear or semi-empirical NDVI models to monitor the vegetation cover changes has attracted growing attention from the scientific community.

The scaling effect of the NDVI cannot be addressed efficiently by image preprocessing techniques; therefore, it has become one of the main issues influencing $f_c$ estimation based on RA algorithms. This issue involves more than the discrepancies among NDVI values derived from different observation scales, e.g., the NDVI of mixed pixels and endmembers within pixels or the NDVI at a fine resolution where the landscape is homogeneous and at a coarse resolution where the landscape is heterogeneous. It also concerns the errors caused by the application of $f_c$ retrieval models at inappropriate scales, e.g., where a model designed for small-scale analysis is applied to a large-scale analysis. Jiang et al. (2006), Zhang et al. (2006), Obata et al. (2012a),Obata et al. (2012b), and Obata and Huete (2014) independently reported that LSMA was applied to the red and NIR bands to explore ways to correct the spatial scaling effect of the NDVI on RA algorithms. According to Zhang et al. (2006), the NDVI mixture model was applicable to estimating $f_c$ on different scales. Obata et al. (2012a) explained the theoretical basis underlying the scaling effect and developed an NDVI-isoline-based linear mixture model, which was an extension of the RA algorithms to rectify the scaling effect in $f_c$ retrievals. A similar analysis was conducted by Jiang et al. (2006), who proposed a scale-invariant index (i.e., the scaled difference vegetation index (SDVI)). The SDVI was calculated according to the formula of the linear NDVI model with the difference vegetation index (DVI) and proved it as a robust approach.

In view of the soil background effects, the optimized soil adjusted vegetation index (OSAVI) and modified soil adjusted vegetation index (MSAVI) were used in lieu of the NDVI (Gonsamo, 2010; Gonsamo and Chen, 2014; Merlin et al., 2010; Tsai et al., 2016), as both of these performed better at minimizing soil background variances (Qi et al., 1994; Rondeaux et al., 1996). Furthermore, the enhanced vegetation index (EVI) was chosen for deriving $f_c$ by Cho et al. (2014), because it can minimize the soil background and atmospheric interference effects. The modified triangular vegetation index (MTVI2) was selected by Liuet al. (2008)as it minimizes the effects of the soil background and leaf chlorophyll, and maintains adequate sensitivity over a wide range of LAI. To address the saturation problem of the NDVI, Li et al. (2014)incorporated the average $f_c$ estimates from the ratio vegetation index (RVI) and NDVI (hereafter denoted NDVI plus RVI) to obtain more accurate results than those yielded by a single VI. The variable atmospherically resistant index (VARI) also performed better than the NDVI in terms of $f_c$ estimation (Jimenez-Munoz et al., 2009). Apart from the aforementioned vegetation indices, other vegetation indices (e.g., vegetation, bare soil, and shadow indices (VBSI) (Zhang et al., 2013)) have also been employed for $f_c$ retrievals using RA algorithms. However, although these vegetation indices were used as substitutes for the NDVI, none of them is as the universal VI that can replace the other sufficiently.

# 4 Overview of RA algorithms

RA algorithms constitute a big branch of remote sensing methods for estimating $f_c$. An overview, including a search and selectionstrategy, literature status, and performance evaluation, is now provided in this section to present the status quo and trends in the development of RA algorithms.

## 4.1 Search and selection strategy

This review is focused specifically on English-language peer-reviewed journal papers published between January 1990 and November 2019 that reported studies in which RA algorithms were applied to estimate $f_c$. Before query processing, we designed two major categories of terms to search the relevant literature: $f_c$-based terms ("fractional vegetation cover" OR "green vegetation fraction" OR "vegetation fraction coverage" OR "canopy fraction cover" OR "fraction of vegetation cover" OR "vegetation cover fraction") and terms related to RA algorithms (("vegetation index" OR "NDVI") OR ("spectral mixture analysis" OR "linear mixture model") OR "scaled NDVI" OR "NDVI SMA" OR "linear NDVI model" OR "dimidiate pixel model" OR "pixel dichotomy model" OR "two-endmember mixing model" OR "quadratic NDVI model")). A TOPIC-based Boolean query search using $f_c$-based terms returned 489 records pertaining to the relevant studies on $f_c$, of which 234 publications also contained terms related to RA algorithms. These records were further screened by investigating thoroughly all the articles to exclude irrelevant studies with similar terms. Finally, 173 studies in which RA algorithms were used to estimate $f_c$ were selected.

To conduct the present review, we derived a set of descriptive statistics from the 173 publications based on the following pre-defined criteria:

**(1)** The linear NDVI model (for the semi-empirical NDVI model) and its analogous versions that employ other vegetation indices as substitutes for NDVI were regarded as linear VI models (for semi-empirical VI models) and then counted. As the formula of the scaled NDVI (see Eq.(10)) is identical to the right hand side of Eq. (6), we regarded the scaled NDVI as a linear VI model.

**(2)** The studies in which multi-sensor images (Qi et al., 2000) or different RA algorithms (Li et al., 2013; Wittich and Hansing, 1995) or both (Montandon and Small, 2008) were used to derive $f_c$ were occasionally divided into sub-studies and considered as individual cases according to the number of remotely sensed image types and corresponding models in the literature.

**(3)** The spatial resolutions (abbreviated as "R") of remote sensing images used to estimate $f_c$ based on the RA algorithms in the selected studies were classified into four types: $R \leq 10$ m; 10 m $< R <$ 100 m; 100 m $\leq R <$ 1 km; and $R \geq 1$ km. It should be noted that images with the same spatial resolution were treated as the same type in a study.

It should also be noted that these statistics are influenced by the study selection process employed in the present review and might lack completeness.

## 4.2 Literature status

**4.2.1 Published trends—**Over the past three decades, RA algorithms have been used in numerous applications as demonstrated by the 173 papers published in 62 academic journals on remote sensing, agriculture, forestry, wetlands, hydrology, and meteorology (Table 2). The top three journals in terms of publications related to the RA algorithms were found to be *Remote Sensing, Remote Sensing of Environment,* and *International Journal of Remote Sensing.* The number of published items (the bar in Fig. 3), as well as the general trend of the usage frequency of the RA algorithms (the broken line in Fig. 3), increased consistently in each five-year time interval between 1990 and 2019. Furthermore, among these RA algorithms, the linear VI model was the most frequently applied followed by the quadratic NDVI model. The NDVI mixture model was rarely used, and has not even been reported in the literature since 2010. The possible explanation, why the linear VI and quadratic NDVI models were more popular, could be related to their considerably simpler formulations as compared to the NDVI mixture model, as well as to the fact that they do not require any additional variables to be calculated, e.g., the extinction coefficient in the semi-empirical VI model.

**4.2.2 Sensor type—**The remote sensing data used in the selected literature were collected mainly from satellite sensors, although in several studies airborne sensor data, ground-based spectroradiometer measurements (e.g., ASD FieldSpecFR spectrometer data and MSR5 field-portable radiometer data), or simulated data were used. In general, the increasing usage of RA algorithms was closely related to the availability of remote sensing data, as well as to the innovations and increasing deployment of remote sensing instruments (Fig. 4). In terms of satellite images, early landmarks in the spatially explicit estimation of $f_c$ using RA algorithms emerged almost 30 years ago through the usage of remote sensing images with low spatial resolution ($R \geq 1$ km, e.g., the Advanced Very High Resolution Radiometer (AVHRR)). Although the higher spatial resolution Landsat Thematic Mapper (TM) satellite data were also collected at that time, they were not yet freely available to the public, which has limited their usage in the research. Despite the growing availability of time series satellite data in the 21st century, moderate-coarse ($100\ m \leq R < 1$ km) and moderate ($10\ m < R < 100$ m) spatial resolutions satellite images became the most frequently employed data sources among those utilized for RA algorithms. The most frequently applied sensor type was the Landsat series (involving TM, Enhanced Thematic Mapper Plus (ETM+), and OLI) data, which was used in 31.9% of the studies, followed by the MODIS data (28.6%). This explains why RA algorithms are focused predominantly on moderate and low spatial resolution ($R > 10$ m) remote sensing applications. Nonetheless, in recent years, increased attention has been paid to the use of high-resolution satellite sensors ($R \leq 10$ m, e.g., IKONOS, SPOT-5/HRG, RapidEye, WorldView-2, and ZY-3). Although there are strong biases depending on sensor type, most studies have made use of multispectral systems, and only a few cases of hyperspectral studies were found in which CASI, OMIS, Hyperion, or HJ-1 A/HIS sensors were used. Furthermore, the dominant image spatial resolutions in $f_c$ estimation using RA algorithms are 30 m, 250 m, and 1 km, which correspond to the Landsat series, MODIS, and AVHRR data, respectively. Consequently, images at these three levels were specially sorted out in terms of the types of RA algorithms used (excluding the NDVI mixture model) (Fig. 5). Images with a 30-m

spatial resolution were most frequently used for $f_c$ estimation after the year 2000, while 1-km AVHRR images were the most frequently used between 1990 and 1999. Additionally, the linear VI model was most frequently applied to images with a 30-m spatial resolution, and the semi-empirical VI model has been rarely used for images with a 250-m, 1-km, and even lower spatial resolutions.

**4.2.3 Geographic patterns and geoscientiflc applications—**Research institutions corresponding to the selected articles are located in 23 countries (Fig. 6), mainly in Asia (accounting for 51%, especially China), followed by North America (24%, especially the United States), and Europe (19%). There has been relatively little research pertaining to the use of RA algorithms in Oceania, South and Central America, and Africa. Among the 173 publications, approximately 49% of the studies focused on the methodological issues, whereas the remainder concerned indirect applications. In particular, researchers in Asia paid more attention to methodological issues and the application of RA algorithms to the estimation of vegetation cover. Conversely, indirect applications have gained wider attention in Europe. In North America, the number of studies form the two aspects is nearly equal. In terms of vegetation types, RA algorithms can be used to determine $f_c$ of varying plant species, such as crops (Liu et al., 2008), grasslands (Rundquist, 2002), forests (Yang et al., 2013), shrubbery (Zhou et al., 2009), desert vegetation (Jiapaer et al., 2011), and even aquatic plants (Cheruiyot et al., 2014).

RA algorithms play an important role in global $f$ estimation (Wuet al., 2014; Zeng et al., 2003) and serve as a feasible means of detecting vegetation recovery in areas that have experienced natural hazards, such as forest fires (Vila and Barbosa, 2010), typhoons (Wang and Xu, 2018), or earthquakes (Jiao et al., 2014). In addition, a large number of research works have assessed the effectiveness of RA algorithms for deriving spatiotemporal distributions of $f_c$ at the regional scale. Fig. 6 shows the geographic locations of their study areas (except for the national- or global-scale studies) as presented in the literature. From Fig. 6, it can be seen that most studies were conducted in China, especially in areas on the northwestern side of the Hu Line (Hu, 1935), including such research sites as Mu Us Sandland (Cao et al., 2011; Liu et al., 2019), the Heihe River basin (Jia et al., 2017; Wang et al., 2014), the Qaidam basin (Jin et al., 2016; Zhang et al., 2019), the Tibetan Plateau (Liu et al., 2014; Wang et al., 2014), and the grasslands of Inner Mongolia (Li et al., 2014; Li et al., 2013). The northwestern side of the Hu Line is sparsely populated, whereas the dense population distribution in China is concentrated predominantly in the southeast; RA algorithms have rarely been applied in the latter. There were also many research sites in Europe, particularly in Spain and Germany (Imukova et al., 2015; Verger et al., 2009). Not many locations in the United States appear in Fig. 6, however, this is mainly because many studies conducted in the United States using RA algorithms were nationwide or global in scale (Gallo et al., 2001; Jiang et al., 2010). In terms of the geographic distribution of regional studies on $f_c$, most of them were conducted in northern temperate zones at latitudes between 25° and 55°N, while less attention was paid to tundra, boreal forest, tropical rain forest, and tropical savanna ecosystems.

In terms of indirect applications utilizing $f_c$ values derived by RA algorithms, related studies included the calculation of land surface parameters such as LAI (Propastin

and Erasmi, 2010; Walthall et al.,2004), M (Vicente-Serrano et al., 2004; Wang et al., 2018), LSE (Sobrino et al., 2008), $T_s$(Agam et al., 2007; Bhattacharya andDadhwal, 2005), ET (Long and Singh, 2012; Tang et al., 2009), SEF (Liet al., 2005; Liu et al., 2017), and IS (Kaspersen et al., 2015). As the NDVI has been used traditionally as an indicator of vegetation abundance to estimate the relationship between surface temperature and vegetation (Petropoulos et al., 2009), RA algorithms were commonly used to determine satellite-derived land surface energy fluxes (including LSE, $T_s$, ET, and SEF) and soil surface moisture analysis. In addition to studies on indirect applications using visible-infrared remote sensing data, both previous and latest studies have reported that combinations of RA algorithms and microwave remote sensing data improved soil moisture retrieval (Hasan et al., 2014) or the disaggregation of $T_s$(Amazirh et al., 2019).

### 4.3 Performance evaluation of RA algorithms

The present study reviewed the performance evaluation of RA algorithms performed in the previous research works in terms of two aspects: comparisons of models within the RA family, and comparing RA algorithms with other $f_c$ estimation approaches.

Numerous studies have attempted to determine which model within the RA family is the most effective in deriving $f_c$ through a comparative analysis of model sensitivity to the soil background (Ding et al., 2017; Montandon and Small, 2008), scale (Jiang et al., 2006), and atmospheric (Gonsamo, 2010) effects. In general, RA algorithms are affected by soil noise mainly because of the sensitivity of VI values to soil optical properties. However, the quadratic NDVI model was found to be superior to the linear NDVI model in terms of reducing soil noise (Dinget al., 2017; Montandon and Small, 2008). In terms of the scale effect, the semi-empirical NDVI and quadratic NDVI models were found to outperform the linear NDVI model, as the former ones transform the scaled NDVI through power functions that reduce the positive bias of the scaled NDVI (Jiang et al., 2006). SDVI was concluded to be scaleinvariant (Jiang et al., 2006) and less sensitive to the atmospheric scattering effects (Gonsamo, 2010). However, SDVI did not perform as well as expected in some applications using moderate and low spatial resolution satellite images (Ding et al., 2016a; Li et al., 2014; Merlin et al., 2010). In addition, several studies also assessed the applicability of various vegetation indices used in RA algorithms to perform $f_c$ estimation. The MSAVI (Wang et al., 2005), VARI (Jimenez-Munoz et al., 2009), NDVI plus RVI (Li et al., 2014), and MTVI2 (Liu et al., 2008) were suggested and confirmed as feasible alternatives to the NDVI.

Many studies also investigated the discrepancies between RA algorithms and other $f_c$ estimation approaches in terms of $f_c$ retrieval. RA algorithms were generally yielded reasonable $f_c$ estimates; however, in areas dominated by NPV (e.g., dry shrubs) and sparse vegetation (e.g., desert plants) they tended to exhibit larger degrees of error compared with other $f_c$ estimation approaches, such as LSMA (Cheruiyot et al., 2014; Xiao and Moody, 2005), multiple endmember spectral mixture analysis (MESMA) (Liu et al., 2017), a combination of geometric-optical models with SMA (Cao et al., 2011), support vector machine (SVM) (Ge et al., 2018), and the modified three-band maximal gradient difference (TGDVI) model (Jiapaer et al., 2011). Additionally, Ding et al. (2016a) reported that the

results yielded by RA algorithms were slightly better than those generated from the look-up table-based inversion of the PROSAIL model and were also faster in terms of computational time.

## 5 RA challenges in relation to the earth system science and future perspectives

### 5.1 Novel approaches for improving RA algorithms

One of the main ways to improve the RA algorithms is to develop or utilize a VI that is highly sensitive to the parameter of interest (i.e., $f_C$), but insensitive to the expected perturbing components (e.g., species, soil, shadow, and non-photosynthetic materials). In this regard, it is possible to consider the modified chlorophyll absorption reflectance index ($MCARI_{(705,750)}$), which uses bandwidths other than those of the traditional broadband VI and is designed to minimize the effects of soil and NPV (Jay et al., 2017; Wu et al., 2008), as a more appropriate alternative to the NDVI. In particular, in the context of the growing amount of freely available Sentinel-2 (S2) databases, as the central wavelengths of the S2 image band 3/5/6 are close to the hyperspectral bands used to calculate $MCARI_{(705,750)}$, the $MCARI_{(705,750)}$-based linear VI model is expected to mitigate the impact of the soil background and non-photosynthetic materials on $f_C$ estimation. However, the relationship between $MCARI_{(705,750)}$ and $f_C$ still requires further evaluation. Kallel et al. (2008) also suggested that fusion of vegetation indices, for example, MCARI/OSAVI (Daughtry et al., 2000), could be an alternative direction to improve their performance. However, the means for rendering this combined VI approach applicable to RA algorithms to yield a more powerful and universal model for retrieving $f_C$ also requires further research. In addition, previous studies (Guerschman et al., 2009; Hill et al., 2016) revealed that the combination of visible, NIR and the shortwave-infrared (SWIR) bands could facilitate the extraction of $f_C$ from pixels composed of green vegetation, bare soil, and the NPV. This motivates development of three-endmember (including photosynthetic vegetation, NPV or shadow, and bare soil) mixing models as an extension of RA algorithms. However, the use of these models implies that sensors must meet higher band setting requirements, i.e., they should be equipped with not only the conventional visible and NIR spectral bands, but also the SWIR bands. Therefore, for satellite sensors having only visible and NIR bands and lacking SWIR bands, further investigation should be focused on how to improve the performance of RA algorithms by overcoming the problem associated with a limited spectral resolution.

In addition to the development of more suitable vegetation indices, the improvement in the accuracy of $VI_{\infty}$ and $VI_s$ estimates by rendering both values less sensitive to plant species and soil background is another future research priority. In this context, the endmember generation algorithm (EGA)—including the minimum volume transform (MVT) (Craig, 1994; Hendrix et al., 2012), non-negative matrix factorization (NMF) (Pauca et al., 2006; Tong et al., 2017), and independent component analysis (ICA) (Chen and Zhang, 1999; Xia et al., 2011)—may be appropriate. The EGA has been used mainly for analyzing hyperspectral remote sensing images; therefore, the issue of effectively using EGA for multispectral images needs to first be addressed.

Furthermore, the fractional cover of green vegetation should be further divided into sunlit and shaded vegetation components because of the difference between sunlit and shaded leaves in terms of absorbed photosynthetically active radiation (PAR). This would be beneficial for optimizing the precision of the light use efficiency models to understand the process of carbon and water cycles of terrestrial ecosystems. Therefore, the development of a simple, available, and robust algorithm based on the formulae of RA algorithms for estimating sunlit and shaded vegetation cover is critically required.

### 5.2 Challenges and future prospects on applications and sensors

As discussed above in Section 4.2.3, RA algorithms have been widely used over the last three decades. Nevertheless, in certain cases associated with LULC changes, such as those where the potential presence of landslides and land flows needs to be inferred (Chen and Huang, 2013), drought conditions need to be quantitatively estimated (Barbosa et al., 2019) and post-fire vegetation recovery monitoring is required (Veraverbeke et al., 2012), very little attention has been paid to the use of RA algorithms. Natural hazards are major threats to human life and the world economy. As is known, rapid and prompt detection of the vegetation cover changes is specifically important for disaster prevention and mitigation and post-disaster recovery (Dahigamuwa et al., 2016; Sekizawa et al., 2015). Specifically, in the face of recurring droughts in arid and semi-arid regions (e.g., southern Africa), detailed spatiotemporal patterns of drought are vital for scheduling agricultural management practices and thus ensuring food security. The modified perpendicular drought index (MPDI) was developed by Ghulam et al., (2007) by introducing the $f_c$ derived by the semi-empirical NDVI model and has been efficiently used for crop drought monitoring. In addition, in view of the frequent fires in the Amazon forest, pragmatic algorithms for monitoring post-fire vegetation recovery efficiently may be helpful for forest management. Vila and Barbosa (2010) demonstrated that post-fire vegetation regrowth detection using the semi-empirical NDVI model was more accurate than that using SMA, although both underestimated $f_c$ (possibly, owing to the presence of the NPV). Therefore, mitigating the NPV effects is a priority for broadening the application of RA algorithms. In this regard, as discussed in Section 5.1, the MCARI($_{70}5_{j7}5_{0}$)-based linear VI model might be more useful for assessing post-fire vegetation recovery.

Focusing on sensor types, we note that RA algorithms have rarely been applied to Sentinel-2 data, which have come to be among the most popular sources of remote sensing data used for the derivation of $f_c$(Verrelst et al., 2012; Wang et al., 2018). Three newly added red-edge wavelength bands of S2, which are not presented in many other satellite sensors, such as the Landsat series, may lead to breakthrough innovations in RA algorithms, because red-edge-based indices were found to be highly correlated with the vegetation cover in previous studies (Gitelson, 2013; Liu et al., 2007). A recent study by Feng et al. (2017)showed that use of the red-edge slope instead of the NDVI in the linear VI and semi-empirical VI models could improve the precision of the retrieved $f_c$ values. In addition, China's high-resolution earth observation system (CHEOS) satellite series also play an important role in longterm remote sensing services (Gu and Tong, 2015). According to Jiaet al. (2016), GF-1 wide field view (WFV) surface reflectance data can produce satisfactory $f_c$ products. However, thus far, only little international attention has been paid to the CHEOS satellite series. In the last

several years, the GaoFen (GF) satellite series (GF-2/-4/-5/-6) were launched successively and have significantly increased the earth observation system's capacity. More recently, the 16-m data of GF-1 and GF-6 can be freely downloaded by users on China National Space Administration (CNSA) GEO platform (access at: http://www.cnsageo.com). Other GF satellite images (e.g., GF-5) are not available as openaccess satellite data, but they are expected to be in the near future. Therefore, the CHEOS satellite series are expected to aid in the near real-time quantitative measurement of vegetation, which could bridge the data gaps in the long revisit cycle of current operating earth resource satellites (e.g., the Landsat series) and could respond to the demand for accurate and prompt $f_c$ estimation. However, development of approaches for harmonizing GF satellite observations to achieve the maximum benefit from current earth observation instruments is a significant challenge. In brief, the S2 data and GF images have extraordinary potential for deriving spatial and temporal distributions of $f_c$. However, the applicability of combinations of such data with RA algorithms for vegetation cover monitoring remains largely unexplored and requires further investigation.

## 6 Conclusions

Given the increasing interest in the exploration of land surfaces, regularly and promptly updated vegetation cover products are essential. This requires convenient and powerful processing methods for quantifying $f_c$. In this review, we discussed the background, issues, status quo and trends, challenges, and future prospects of RA algorithms based on 173 selected scientific publications. The most important key findings are listed below:

**(1)** The number of studies using RA algorithms has increased constantly over the last three decades, and the linear VI model has been the most frequently used within the RA family. The Landsat series and MODIS remain the most frequently used data sources for the $f_c$ estimation using RA algorithms, although the most recent studies have focused increasingly on the use of high-resolution satellite data from other spaceborne sensors. Regional studies of $f_c$ have been conducted mainly in the northern temperate zones at latitudes between 25° and 55°N, whereas regional studies that include Oceania, South/Central America, and Africa were presented limitedly.

**(2)** In the related research, three main issues influencing the inversion accuracy of $f_c$ using RA algorithms are to determine $NDVI_\infty$ and $NDVI_s$ values, to correct for the inherent limitations of NDVI, and to mitigate the NPV effects. For large-scale applications, we recommend the use of the improved methods proposed by Zeng et al. (2000), Montandon and Small (2008), Song et al. (2017), and Muet al. (2018). We also emphasize the importance of evaluating the performance of these improved methods using remote sensing images with other spatial resolutions, in addition to the Landsat and MODIS data. In addition, the MSAVI, VARI, NDVI plus RVI, and MTVI2 could be feasible alternatives to the NDVI in RA algorithms for $f_c$ estimation. We recommend that future research considers the substitution of NDVI by red-edge vegetation indices (e.g.,

$MCARI_{(705,750)}$) and utilizes the new generation of satellite sensors (e.g., S2, CHEOS satellites) for near real-time retrieval of $f_c$.

## Acknowledgements

This work was partly supported by the National Natural Science Foundation of China (No. 41771370, 41871230), the National Key Research and Development Program of China (No. 2017YFD0600903, 2018YFA0605503), and the High-resolution Earth Observation Project of China (No. 03-Y20A04-9001-17/18, 30-Y20A07-9003-17/18). The first author especially acknowledges the tremendous amount of feedback of Dr. Xubin Zeng which has greatly improved the paper. We thank Dr. Lixia Ma and Dr. Yan Huang who read the early version of this study. Finally, we would like to provide our great gratitude to anonymous reviewers and members of the editorial team for their helpful and valuable comments that was of great help to increase the quality of the manuscript.

## References

Adams JB, Smith MO, Johnson PE. Spectral mixture modeling – a new analysis of rock and soil types at the viking lander-1 site. J Geophys Res-Solid Earth Planets. 1986; 91: 8098–8112.

Agam N, Kustas WP, Anderson MC, Li F, Neale CMU. A vegetation indexbased technique for spatial sharpening of thermal imagery. Remote Sens Environ. 2007; 107: 545–558.

Allen RG, Pereira LS. Estimating crop coefficients from fraction of ground coverand height. Irrig Sci. 2009; 28: 17–34.

Amazirh A, Merlin O, Er-Raki S. Including Sentinel-1 radar data to improve thedisaggregation of MODIS land surface temperature data. ISPRS J Photogramm Remote Sens. 2019; 150: 11–26.

Asrar G, Fuchs M, Kanemasu ET, Hatfield JL. Estimating absorbed photosynthetic radiation and leaf-area index from spectral reflectance in wheat. Agron J. 1984; 76: 300–306.

Barbosa HA, Kumar TL, Paredes F, Elliott S, Ayuga JG. Assessment of Caatinga response to drought using Meteosat-SEVIRI normalized difference vegetation index (2008–2016). ISPRS J Photogramm Remote Sens. 2019; 148: 235–252.

Baret F, Clevers J, Steven MD. The robustness of canopy gap fraction estimatesfrom red and near-infrared reflectances – a comparison of approaches. Remote Sens Environ. 1995; 54: 141–151.

Baret F, Guyot G. Potentials and limits of vegetation indexes for LAI and APAR assessment. Remote Sens Environ. 1991; 35: 161–173.

Best RG, Harlan JC. Spectral estimation of green leaf-area index of oats. Remote Sens Environ. 1985; 17: 27–36.

Bhattacharya BK, Dadhwal VK. Land surfaace temperature retrieval and itsvalidation using NOAA AVHRR thermal data. J Indian Soc Remote Sens. 2005; 33: 331–338.

Broxton PD, Zeng X, Scheftic W, Troch PA. A MODIS-based global 1-kmmaximum green vegetation fraction dataset. J Appl Meteor Climatol. 2014; 53: 1996–2004.

Cao C, Chen W, Li G, Jia H, Ji W, Xu M, Gao M, Ni X, Zhao J, Zheng S, Tian R, et al. The retrieval of shrub fractional cover based on a geometric-optical model in combination with linear spectral mixture analysis. Can J Remote Sens. 2011; 37: 348–358.

Carlson TN, Ripley DA. On the relation between NDVI, fractional vegetation cover, and leaf area index. Remote Sens Environ. 1997; 62: 241–252.

Chen CY, Huang WL. Land use change and landslide characteristics analysis forcommunity-based disaster mitigation. Environ Monit Assess. 2013; 185: 4125–4139. [PubMed: 22961329]

Chen, CH, Zhang, XH. Image and Signal Processing for Remote Sensing V. Serpico, SB, editor. Spie-Int Soc Optical Engineering; Bellingham: 1999. 150–158.

Cheruiyot EK, Mito C, Menenti M, Gorte B, Koenders R, Akdim N. Evaluating MERIS-based aquatic vegetation mapping in Lake Victoria. Remote Sens. 2014; 6: 7762–7782.

Cho J, Lee Y-W, Han K-S. The effect of fractional vegetation cover on therelationship between EVI and soil moisture in non-forest regions. Remote Sens Lett. 2014; 5: 37–45.

Chopping M, Su L, Rango A, Martonchik JV, Peters DPC, Laliberte A. Remote sensing of woody shrub cover in desert grasslands using MISR with a geometric-optical canopy reflectance model. Remote Sens Environ. 2008; 112: 19–34.





Europe PMC Funders Author Manuscripts

Choudhury BJ, Ahmed NU, Idso SB, Reginato RJ, Daughtry CST. Relations between evaporation coefficients and vegetation indexes studied by model simulations. Remote Sens Environ. 1994; 50: 1–17.

Craig MD. Minimum-volume transforms for remotely-sensed data. IEEE Trans Geosci Remote Sens. 1994; 32: 542–552.

Dahigamuwa T, Yu Q, Gunaratne M. Feasibility study of land cover classification based on normalized difference vegetation index for landslide risk assessment. Geosciences. 2016; 6: 45.

Daughtry C, Walthall C, Kim M, De Colstoun EB, McMurtrey Iii J. Estimatingcorn leaf chlorophyll concentration from leaf and canopy reflectance. Remote Sens Environ. 2000; 74: 229–239.

de la Casa A, Ovando G, Bressanini L, Martinez J, Diaz G, Miranda C. Soybean crop coverage estimation from NDVI images with different spatial resolutionto evaluate yield variability in a plot. ISPRS J Photogramm Remote Sens. 2018; 146: 531–547.

Deardorff JW. Efficient prediction of ground surface-temperature and moisture,with inclusion of a layer of vegetation. J Geophys Res-Oceans. 1978; 83: 1889–1903.

Ding Y, Zhang H, Li Z, Xin X, Zheng X, Zhao K. Comparison of fractional vegetation cover estimations using dimidiate pixel models and look-up table inversions of the PROSAIL model from Landsat 8 OLI data. J Appl Remote Sens. 2016a; 10 036022

Ding Y, Zhang H, Zhao K, Zheng X. Investigating the accuracy of vegetation index-based models for estimating the fractional vegetation cover and the effects of varying soil backgrounds using in situ measurements and the PROSAIL model. Int J Remote Sens. 2017; 38: 4206–4223.

Ding Y, Zheng X, Zhao K, Xin X, Liu H. Quantifying the impact of NDVIsoil determination methods and NDVIsoil variability on the estimation of fractional vegetation cover in northeast China. Remote Sens. 2016b; 8: 29.

Feng H, Feng Z, Feng H. A new method for estimating the fractional vegetation cover based on UVA hyperspectrum. Spectrosc Spectral Anal. 2017; 37: 3573–3578.

Foley JA, Levis S, Costa MH, Cramer W, Pollard D. Incorporating dynamic vegetation cover within global climate models. Ecol Appl. 2000; 10: 1620–1632.

Friedl MA, McIver DK, Hodges JCF, Zhang XY, Muchoney D, Strahler AH, Woodcock CE, Gopal S, Schneider A, Cooper A, Baccini A, et al. Global land cover mapping from MODIS: algorithms and early results. Remote Sens Environ. 2002; 83: 287–302.

Gallo K, Tarpley D, Mitchell K, Csiszar I, Owen T, Reed B. Monthly fractional green vegetation cover associated with land cover classes of the conterminous USA. Geophys Res Lett. 2001; 28: 2089–2092.

Ge J, Meng B, Liang T, Feng Q, Gao J, Yang S, Huang X, Xie H. Modeling alpine grassland cover based on MODIS data and support vector machine regressionin the headwater region of the Huanghe River, China. Remote Sens Environ. 2018; 218: 162–173.

Ge J, Qi J, Lofgren B. Use of vegetation properties from EOS observations for land-climate modeling in East Africa. J Geophys Res-Atmospheres. 2008; 113 D15101

Ghulam A, Qin Q, Teyip T, Li ZL. Modified perpendicular drought index(MPDI): a real-time drought monitoring method. ISPRS J Photogramm Remote Sens. 2007; 62: 150–164.

Gillies RR, Carlson TN. Thermal remote sensing of surface soil water content with partial vegetation cover for incorporation into climate models. J Appl Meteor. 1995; 34: 745–756.

Gillies RR, Carlson TN, Cui J, Kustas WP, Humes KS. A verification of the ‘triangle’ method for obtaining surface soil water content and energy fluxes from remote measurements of the Normalized Difference Vegetation Index (NDVI) andsurface radiant temperature. 1997; Int J Remote Sens. 18: 3145–3166.

Gitelson AA. Remote estimation of crop fractional vegetation cover: the use ofnoise equivalent as an indicator of performance of vegetation indices. Int J Remote Sens. 2013; 34: 6054–6066.

Gonsamo A. Leaf area index retrieval using gap fractions obtained from high resolution satellite data: Comparisons of approaches, scales and atmospheric effects. Int J Appl Earth Obs Geoinf. 2010; 12: 233–248.

Gonsamo A, Chen JM. Continuous observation of leaf area index at Fluxnet-Canada sites. Agric For Meteorol. 2014; 189: 168–174.

Gu XF, Tong XD. Overview of China earth observation satellite programs. IEEE Geosci Remote Sens Mag. 2015; 3: 113–129.

Guan K, Wood EF, Caylor KK. Multi-sensor derivation of regional vegetation fractional cover in Africa. Remote Sens Environ. 2012; 124: 653–665.

Guerschman JP, Hill MJ, Renzullo LJ, Barrett DJ, Marks AS, Botha EJ. Estimating fractional cover of photosynthetic vegetation, non-photosynthetic vegetation and bare soil in the Australian tropical savanna region upscaling the EO-1 Hyperion and MODIS sensors. Remote Sens Environ. 2009; 113: 928–945.

Gutman G, Ignatov A. Satellite-derived green vegetation fraction for the use innumerical weather prediction models. Adv Space Res. 1997; 19: 477–480.

Gutman G, Ignatov A. The derivation of the green vegetation fraction from NOAA/AVHRR data for use in numerical weather prediction models. Int J Remote Sens. 1998; 19: 1533–1543.

Hasan S, Montzka C, Rüdiger C, Ali M, Bogena HR, Vereecken H. Soilmoisture retrieval from airborne L-band passive microwave using high resolution multispectral data. ISPRS J Photogramm Remote Sens. 2014; 91: 59–71.

Hatfield JL, Asrar G, Kanemasu ET. Intercepted photosynthetically active radiation estimated by spectral reflectance. Remote Sens Environ. 1984; 14: 65–75.

Hendrix EMT, Garcia I, Plaza J, Martin G, Plaza A. A new minimum-volume enclosing algorithm for endmember identification and abundance estimation in hyperspectral data. IEEE Trans Geosci Remote Sens. 2012; 50: 2744–2757.

Hill MJ, Zhou Q, Sun QS, Schaaf CB, Southworth J, Mishra NB, Gibbes C, Bunting E, Christiansen TB, Crews KA. Dynamics of the relationship between NDVI and SWIR32 vegetation indices in southern Africa: implications for retrieval of fractional cover from MODIS data. Int J Remote Sens. 2016; 37: 1476–1503.

Huanyong, Hu. The distribution of population in China, with statistics and maps. Acta Geogr Sin. 1935; 2 (2) 33–74.

Imukova K, Ingwersen J, Streck T. Determining the spatial and temporal dynamics of the green vegetation fraction of croplands using high-resolution RapidEye satellite images. Agric For Meteorol. 2015; 206: 113–123.

Jay S, Gorretta N, Morel J, Maupas F, Bendoula R, Rabatel G, Dutartre D, Comar A, Baret F. Estimating leaf chlorophyll content in sugar beet canopies using millimeter- to centimeter-scale reflectance imagery. Remote Sens Environ. 2017; 198: 173–186.

Jia K, Li Y, Liang S, Wei X, Yao Y. Combining estimation of green vegetation fraction in an arid region from Landsat 7 ETM+ data. Remote Sens. 2017; 9: 1121.

Jia K, Liang SL, Gu XF, Baret F, Wei XQ, Wang XX, Yao YJ, Yang LQ, Li YW. Fractional vegetation cover estimation algorithm for Chinese GF-1 widefield view data. Remote Sens Environ. 2016; 177: 184–191.

Jia K, Yao Y, Wei X, Gao S, Jiang B, Zhao X. A review on fractional vegetation cover estimation using remote sensing. Adv Earth Sci. 2013; 28: 774–782.

Jiang L, Kogan FN, Guo W, Tarpley JD, Mitchell KE, Ek MB, Tian Y, Zheng W, Zou CZ, Ramsay BH. Real-time weekly global green vegetation fraction derived from advanced very high resolution radiometer-based NOAA operational global vegetation index (GVI) system. J Geophys Res-Atmospheres. 2010; 115

Jiang M, Tian S, Zheng Z, Zhan Q, He Y. Human activity influences on vegetation cover changes in Beijing, China, from 2000 to 2015. Remote Sens. 2017; 9: 271.

Jiang ZY, Huete AR, Chen J, Chen YH, Li J, Yan GJ, Zhang XY. Analysis of NDVI and scaled difference vegetation index retrievals of vegetation fraction. Remote Sens Environ. 2006; 101: 366–378.

Jiao Q, Zhang B, Liu L, Li Z, Yue Y, Hu Y. Assessment of spatio-temporal variations in vegetation recovery after the Wenchuan earthquake using Landsat data. Nat Hazards. 2014; 70: 1309–1326.

Jiapaer G, Chen X, Bao A. A comparison of methods for estimating fractionalvegetation cover in arid regions. Agric For Meteorol. 2011; 151: 1698–1710.

Jimenez-Munoz JC, Sobrino JA, Plaza A, Guanter L, Moreno J, Martinez P. Comparison between fractional vegetation cover retrievals from vegetation indices and spectral mixture analysis: case

study of PROBA/CHRIS data over an agricultural area. Sensors. 2009; 9: 768–793. [PubMed: 22399938]

Jin X, Liu J, Wang S, Xia W. Vegetation dynamics and their response to groundwater and climate variables in Qaidam Basin, China. Int J Remote Sens. 2016; 37: 710–728.

Jing X, Yao WQ, Wang JH, Sonb XY. A study on the relationship between dynamic change of vegetation coverage and precipitation in Beijing's mountainous areas during the last 20 years. Math Comput Modell. 2011; 54: 1079–1085.

Johnson B, Tateishi R, Kobayashi T. Remote sensing of fractional green vegetation cover using spatially-interpolated endmembers. Remote Sens. 2012; 4: 2619–2634.

Kallel A, Le Hegarat-Mascle S, Hubert-Moy L, Ottle C. Fusion of vegetation indices using continuous belief functions and cautious-adaptive combination rule. IEEE Trans Geosci Remote Sens. 2008; 46: 1499–1513.

Kaspersen PS, Fensholt R, Drews M. Using Landsat vegetation indices to estimate impervious surface fractions for European cities. Remote Sens. 2015; 7: 8224–8249.

Kuang W, Dou Y, Zhang C, Chi W, Liu A, Liu Y, Zhang R, Liu J. Quantifying the heat flux regulation of metropolitan land use/land cover components by coupling remote sensing modeling with in situ measurement. J Geophys Res-Atmospheres. 2015; 120: 113–130.

Li F, Chen W, Zeng Y, Zhao Q, Wu B. Improving estimates of grassland fractional vegetation cover based on a pixel dichotomy model: a case study in Inner Mongolia. China Remote Sens. 2014; 6: 4705–4722.

Li FQ, Kustas WP, Prueger JH, Neale CMU, Jackson TJ. Utility of remote sensing-based two-source energy balance model under low- and high-vegetation cover conditions. J Hydrometeor. 2005; 6: 878–891.

Li XB, Long HL, Wang H. Vegetation cover estimation based on in-suit hy-perspectral data: a case study for meadow steppe vegetation in Inner Mongolia, China. Int J Agric Biol. 2013; 15: 285–290.

Li X, Zhang J. Derivation of the green vegetation graction of the whole China from 2000 to 2010 from MODIS data. Earth Interact. 2016; 20: 1–16. [PubMed: 30026656]

Liu B, Shen W, Lin N, Li R, Yue Y. Deriving vegetation fraction information for the alpine grassland on the Tibetan Plateau using in situ spectral data. J Appl Remote Sens. 2014; 8 083630

Liu JG, Miller JR, Haboudane D, Pattey E, Hochheim K. Crop fraction estimation from casi hyperspectral data using linear spectral unmixing and vegetationindices. Can J Remote Sens. 2008; 34: S124–S138.

Liu K, Su H, Li X. Comparative assessment of two vegetation fractional cover estimating methods and their impacts on modeling urban latent heat flux using Landsat imagery. Remote Sens. 2017; 9: 455.

Liu Q, Zhang T, Li Y, Li Y, Bu C, Zhang Q. Comparative analysis of fractional vegetation cover estimation based on multi-sensor data in a semi-arid sandy area. Chin Geogra Sci. 2019; 29: 166–180.

Liu ZY, Huang JF, Wu XH, Dong YP. Comparison of vegetation indices and red-edge parameters for estimating grassland cover from canopy reflectance data. J Integr Plant Biol. 2007; 49: 299–306.

Long D, Singh VP. A two-source trapezoid model for evapotranspiration (TTME) from satellite imagery. Remote Sens Environ. 2012; 121: 370–388.

Merlin O, Al Bitar A, Walker JP, Kerr Y. An improved algorithm for disaggregating microwave-derived soil moisture based on red, near-infrared andthermal-infrared data. Remote Sens Environ. 2010; 114: 2305–2316.

Miller J, Barlage M, Zeng X, Wei H, Mitchell K, Tarpley D. Sensitivity of the NCEP/Noah land surface model to the MODIS green vegetation fraction data set. Geophys Res Lett. 2006; 33

Montandon LM, Small EE. The impact of soil reflectance on the quantification of the green vegetation fraction from NDVI. Remote Sens Environ. 2008; 112: 1835–1845.

Mu X, Song W, Gao Z, McVicar TR, Donohue RJ, Yan G. Fractional vegetation cover estimation by using multi-angle vegetation index. Remote Sens Environ. 2018; 216: 44–56.

Nilson T. A theoretical analysis of frequency of gaps in plant stands. Agric Meteorol. 1971; 8: 25–38.

Obata K, Huete AR. Scaling effects on area-averaged fraction of vegetation cover derived using a linear mixture model with two-band spectral vegetation index constraints. J Appl Remote Sens. 2014; 8 083629

Obata K, Miura T, Yoshioka H. Analysis of the scaling effects in the area-averaged fraction of vegetation cover retrieved using an NDVI-isoline-based linearmixture model. Remote Sens. 2012a; 4: 2156–2180.

Obata K, Wada T, Miura T, Yoshioka H. Scaling effect of area-averaged NDVI: monotonicity along the spatial resolution. Remote Sens. 2012b; 4: 160–179.

Okin GS, Clarke KD, Lewis MM. Comparison of methods for estimation of absolute vegetation and soil fractional cover using MODIS normalized BRDF-adjusted reflectance data. Remote Sens Environ. 2013; 130: 266–279.

Pauca VP, Piper J, Plemmons RJ. Nonnegative matrix factorization for spectral data analysis. Linear Alg Appl. 2006; 416: 29–47.

Petropoulos G, Carlson T, Wooster M, Islam S. A review of Ts/VI remote sensing based methods for the retrieval of land surface energy fluxes and soil surface moisture. Prog Phys Geogr. 2009; 33: 224–250.

Price JC. Using spatial context in satellite data to infer regional scale evapo-transpiration. IEEE Trans Geosci Remote Sens. 1990; 28: 940–948.

Propastin P, Erasmi S. A physically based approach to model LAI from MODIS 250 m data in a tropical region. Int J Appl Earth Obs Geoinf. 2010; 12: 47–59.

Qi J, Chehbouni A, Huete A, Kerr Y, Sorooshian S. A modified soil adjusted vegetation index. Remote Sens Environ. 1994; 48: 119–126.

Qi J, Marsett RC, Moran MS, Goodrich DC, Heilman P, Kerr YH, Dedieu G, Chehbouni A, Zhang XX. Spatial and temporal dynamics of vegetation in the San Pedro River basin area. Agric For Meteorol. 2000; 105: 55–68.

Refslund J, Dellwik E, Hahmann AN, Barlage MJ, Boegh E. Development of satellite green vegetation fraction time series for use in mesoscale modeling: application to the European heat wave 2006. Theor Appl Climatol. 2014; 117: 377–392.

Roberts DA, Gardner M, Church R, Ustin S, Scheer G, Green RO. Mapping chaparral in the Santa Monica Mountains using multiple endmember spectral mixture models. Remote Sens Environ. 1998; 65: 267–279.

Rondeaux G, Steven M, Baret F. Optimization of soil-adjusted vegetation indices. Remote Sens Environ. 1996; 55: 95–107.

Rundquist BC. The influence of canopy green vegetation fraction on spectral measurements over native tallgrass prairie. Remote Sens Environ. 2002; 81: 129–135.

Scheftic W, Zeng X, Broxton P, Brunke M. Intercomparison of seven NDVI products over the United States and Mexico. Remote Sens. 2014; 6: 1057–1084.

Sekizawa R, Ichii K, Kondo M. Satellite-based detection of evacuation-induced land cover changes following the Fukushima Daiichi nuclear disaster. Remote Sens Lett. 2015; 6: 824–833.

Settle JJ, Drake NA. Linear mixing and the estimation of ground cover proportions. Int J Remote Sens. 1993; 14: 1159–1177.

Sobrino JA, Jimenez-Munoz JC, Soria G, Romaguera M, Guanter L, Moreno J, Plaza A, Martincz P. Land surface emissivity retrieval from different VNIR and TIR sensors. IEEE Trans Geosci Remote Sens. 2008; 46: 316–327.

Song W, Mu X, Ruan G, Gao Z, Li L, Yan G. Estimating fractional vegetation cover and the vegetation index of bare soil and highly dense vegetation with aphysically based method. Int J Appl Earth Obs Geoinf. 2017; 58: 168–176.

Stojanova D, Panov P, Gjorgjioski V, Kohler A, Dzeroski S. Estimating vegetation height and canopy cover from remotely sensed data with machine learning. Ecol Inform. 2010; 5: 256–266.

Tang Q, Peterson S, Cuenca RH, Hagimoto Y, Lettenmaier DP. Satellite based near-real-time estimation of irrigated crop water consumption. J Geophys Res-Atmospheres. 2009; 114

Tong L, Zhou J, Li X, Qian YT, Gao YS. Region-based structure preserving nonnegative matrix factorization for hyperspectral unmixing. IEEE J Sel Top Appl Earth Obs Remote Sens. 2017; 10: 1575–1588.

Tong S, Zhang J, Ha S, Lai Q, Ma Q. Dynamics of fractional vegetation coverage and its relationship with climate and human activities in Inner Mongolia, China. Remote Sens. 2016; 8: 776.

Tsai YH, Stow D, Shi L, Lewison R, An L. Quantifying canopy fractional cover and change in Fanjingshan National Nature Reserve, China using multi-temporal Landsat imagery. Remote Sens Lett. 2016; 7: 671–680.

Valor E, Caselles V. Mapping land surface emissivity from NDVI: application to European, African, and South American areas. Remote Sens Environ. 1996; 57: 167–184.

Vegas Galdos F, Alvarez C, Garcia A, Revilla JA. Estimated distributed rainfall interception using a simple conceptual model and Moderate Resolution Imaging Spectroradiometer (MODIS). J Hydrol. 2012; 468: 213–228.

Veraverbeke S, Gitas I, Katagis T, Polychronaki A, Somers B, Goossens R. Assessing post-fire vegetation recovery using red–near infrared vegetation indices: accounting for background and vegetation variability. ISPRS J Photogramm Remote Sens. 2012; 68: 28–39.

Verger A, Martinez B, Camacho-de Coca F, Garcia-Haro FJ. Accuracy assessment of fraction of vegetation cover and leaf area index estimates from pragmatic methods in a cropland area. Int J Remote Sens. 2009; 30: 2685–2704.

Verrelst J, Munoz J, Alonso L, Delegido J, Rivera JP, Camps-Valls G, Moreno J. Machine learning regression algorithms for biophysical parameter retrieval: opportunities for Sentinel-2 and -3. Remote Sens Environ. 2012; 118: 127–139.

Verstraete, MM, Pinty, B. Vegetation and Climate Interactions in Semi-Arid Regions. Henderson-Sellers, A, Pitman, AJ, editors. Springer; Dordrecht: 1991. 59–72.

Vicente-Serrano SM, Pons-Fernandez X, Cuadrat-Prats JM. Mapping soil moisture in the central Ebro river valley (northeast Spain) with Landsat and NOAA satellite imagery: a comparison with meteorological data. Int J Remote Sens. 2004; 25: 4325–4350.

Vila JPS, Barbosa P. Post-fire vegetation regrowth detection in the Deiva Marina region (Liguria-Italy) using Landsat TM and ETM plus data. Ecol Modell. 2010; 221: 75–84.

Walthall C, Dulaney W, Anderson M, Norman J, Fang HL, Liang SL. A comparison of empirical and neural network approaches for estimating corn and soybean leaf area index from Landsat ETM+ imagery. Remote Sens Environ. 2004; 92: 465–474.

Wang B, Jia K, Liang SL, Xie XH, Wei XQ, Zhao X, Yao YJ, Zhang XT. Assessment of Sentinel-2 MSI spectral band reflectances for estimating fractional vegetation cover. Remote Sens. 2018a; 10: 1927.

Wang C, Qi J. Biophysical estimation in tropical forests using JERS-1 VNIR imagery. I: leaf area index. Int J Remote Sens. 2008; 29: 6811–6826.

Wang C, Qi J, Cochrane M. Assessment of tropical forest degradation with canopy fractional cover from landsat ETM plus and IKONOS imagery. Earth Interact. 2005; 9: 1–18.

Wang GX, Liu GS, Li CJ, Yang Y. The variability of soil thermal and hydrological dynamics with vegetation cover in a permafrost region. Agric For Meteorol. 2012; 162: 44–57.

Wang M, Xu H. Remote sensing-based assessment of vegetation damage by a strong typhoon (Meranti) in Xiamen Island, China. Nat Hazards. 2018; 93: 1231–1249.

Wang X, Sun Z, Zhou A-G. Alpine cold vegetation response to climate change in the western Nyainqentanglha range in 1972–2009. Sci World J. 2014; 2014

Wang Y, Peng J, Song X, Leng P, Ludwig R, Loew A. Surface soil moisture retrieval using optical/thermal infrared remote sensing data. IEEE Trans Geosci Remote Sens. 2018b; 56: 5433–5442.

Wang Y, Roderick ML, Shen Y, Sun F. Attribution of satellite-observed vegetation trends in a hyper-arid region of the Heihe River basin, western China. Hydrol Earth Syst Sci. 2014b; 18: 3499–3509.

Wei XH, Li Q, Zhang MF, Giles-Hansen K, Liu WF, Fan HB, Wang Y, Zhou GY, Piao SL, Liu SR. Vegetation cover-another dominant factor in determining global water resources in forested regions. Glob Change Biol. 2018; 24: 786–795.

Wiegand CL, Gerbermann AH, Gallo KP, Blad BL, Dusek D. Multisite analyses of spectral biophysical data for corn. Remote Sens Environ. 1990; 33: 1–16.

Wittich KP. Some simple relationships between land-surface emissivity, greenness and the plant cover fraction for use in satellite remote sensing. Int J Biometeorol. 1997; 41: 58–64.

Wittich KP, Hansing O. Area-averaged vegetative cover fraction estimated from satellite data. Int J Biometeorol. 1995; 38: 209–215.

Wu CY, Niu Z, Tang Q, Huang WJ. Estimating chlorophyll content from hyperspectral vegetation indices: Modeling and validation. Agric For Meteorol. 2008; 148: 1230–1241.

Wu D, Wu H, Zhao X, Zhou T, Tang B, Zhao W, Jia K. Evaluation of spatiotemporal variations of global fractional vegetation cover based on GIMMS NDVI data from 1982 to 2011. Remote Sens. 2014; 6: 4217–4239.

Xia W, Liu XS, Wang B, Zhang LM. Independent component analysis for blind unmixing of hyperspectral imagery with additional constraints. IEEE Trans Geosci, Remote Sens. 2011; 49: 2165–2179.

Xiao JF, Moody A. A comparison of methods for estimating fractional green vegetation cover within a desert-to-upland transition zone in central New Mexico, USA. Remote Sens Environ. 2005; 98: 237–250.

Xiao ZQ, Wang TT, Liang SL, Sun R. Estimating the fractional vegetation cover from GLASS leaf area index product. Remote Sens. 2016; 8: 19.

Xin ZB, Xu JX, Zheng W. Spatiotemporal variations of vegetation cover on the Chinese Loess Plateau (1981–2006): impacts of climate changes and human activities. Sci China Ser D-Earth Sci. 2008; 51: 67–78.

Yang GJ, Pu RL, Zhang JX, Zhao CJ, Feng HK, Wang JH. Remote Sensing of seasonal variability of fractional vegetation cover and its object-based spatial pattern analysis over mountain areas. ISPRS J Photogramm Remote Sens. 2013; 77: 79–93.

Zeng XB, Dickinson RE, Walker A, Shaikh M, DeFries RS, Qi JG. Derivation and evaluation of global 1-km fractional vegetation cover data for land modeling. J Appl Meteor. 2000; 39: 826–839.

Zeng XB, Rao P, DeFries RS, Hansen MC. Interannual variability and decadal trend of global fractional vegetation cover from 1982 to 2000. J Appl Meteor. 2003; 42: 1525–1530.

Zhang F, Tiyip T, Ding J, Sawut M, Johnson VC, Tashpolat N, Gui D. Vegetation fractional coverage change in a typical oasis region in Tarim River Watershed based on remote sensing. J Arid Land. 2013; 5: 89–101.

Zhang S, Chen H, Fu Y, Niu H, Yang Y, Zhang B. Fractional vegetation cover estimation of different vegetation types in the Qaidam Basin. Sustainability. 2019; 11: 864.

Zhang X, Yan G, Li Q, Li ZL, Wan H, Guo L. Evaluating the fraction of vegetation cover based on NDVI spatial scale correction model. Int J Remote Sens. 2006; 27: 5359–5372.

Zhou X, Guan H, Xie H, Wilson JL. Analysis and optimization of NDVI definitions and areal fraction models in remote sensing of vegetation. Int J Remote Sens. 2009; 30: 721–751.



Europe PMC Funders Author Manuscripts

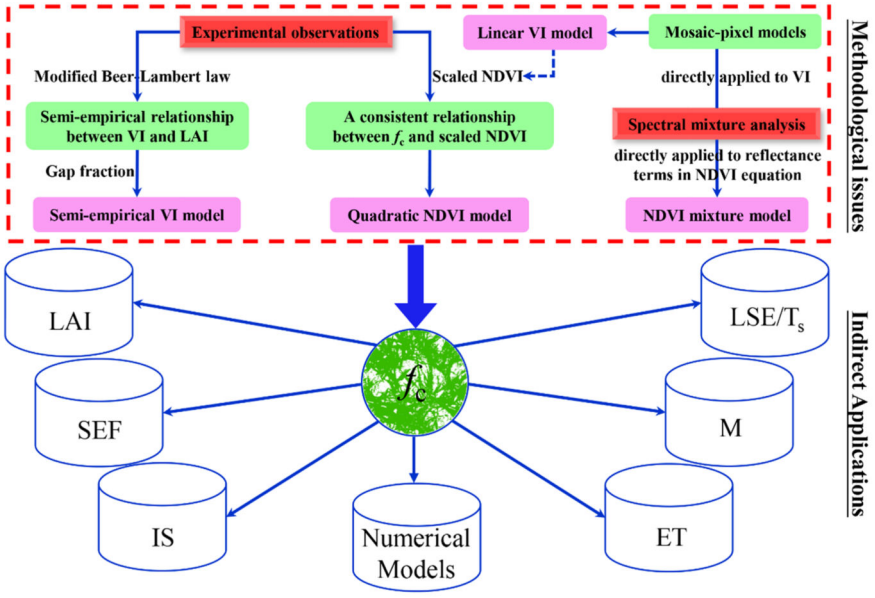


**Fig. 1.**

Summary of the origin, improvement, and applications of relative vegetation abundance algorithms. Numerical models include meteorological, climate, ecohydrological, and agronomic models, and others.





Europe PMC Funders Author Manuscripts

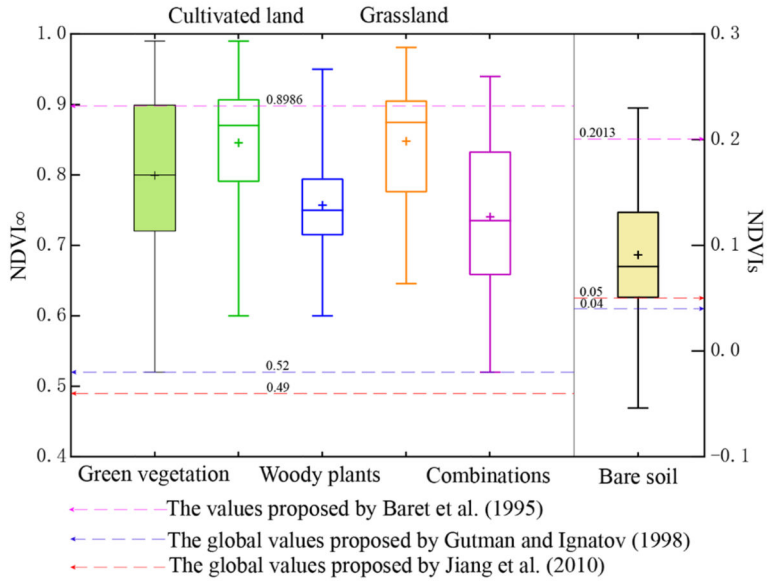


**Fig. 2.**

Values of $NDVI_{\infty}$ and $NDVI_s$. Green vegetation consists of cultivated land, woody plants, grassland, and combinations. Woody plants is a combination of forest and shrubbery. Combinations refers to mixtures of cultivated land, woody plants, and grasslands.




Europe PMC Funders Author Manuscripts

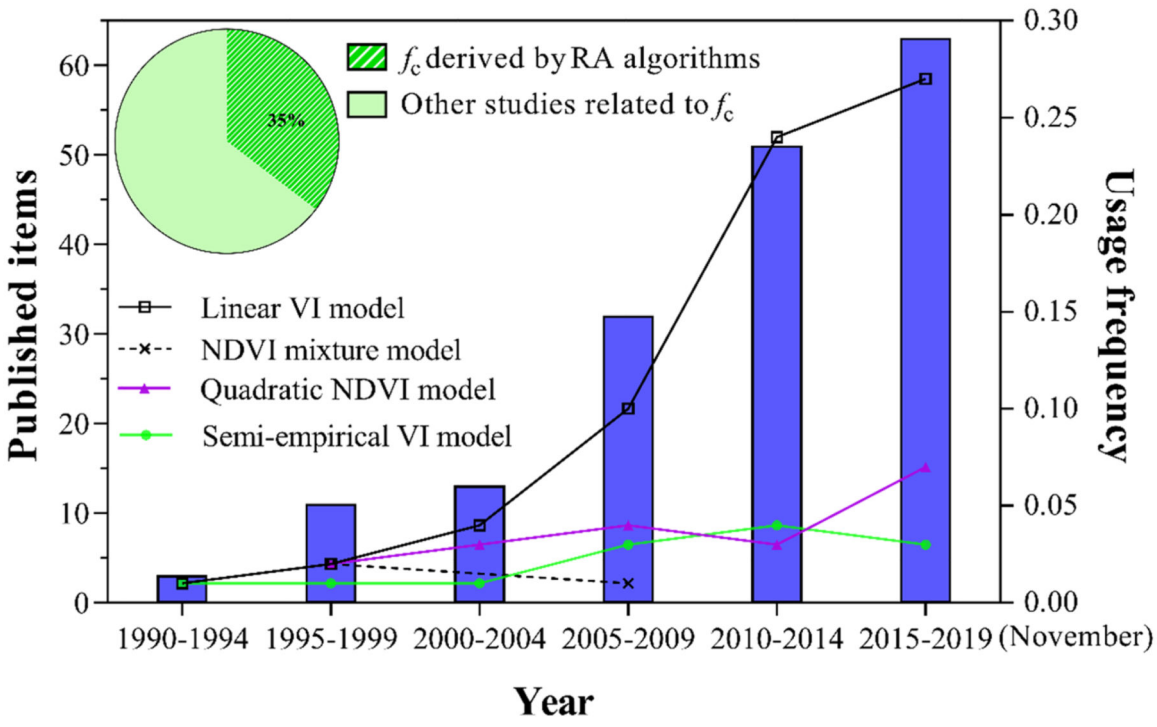


**Fig. 3.**

Published items (left y-axis) and usage frequency (right y-axis) of RA algorithms over the five-year intervals between 1990 and November 2019 (x-axis). The pie chart indicates the contribution of RA algorithms used to estimate $f_c$ in the relevant studies on $f_c$. The broken line shows the trend of usage frequency of RA algorithms.




Europe PMC Funders Author Manuscripts

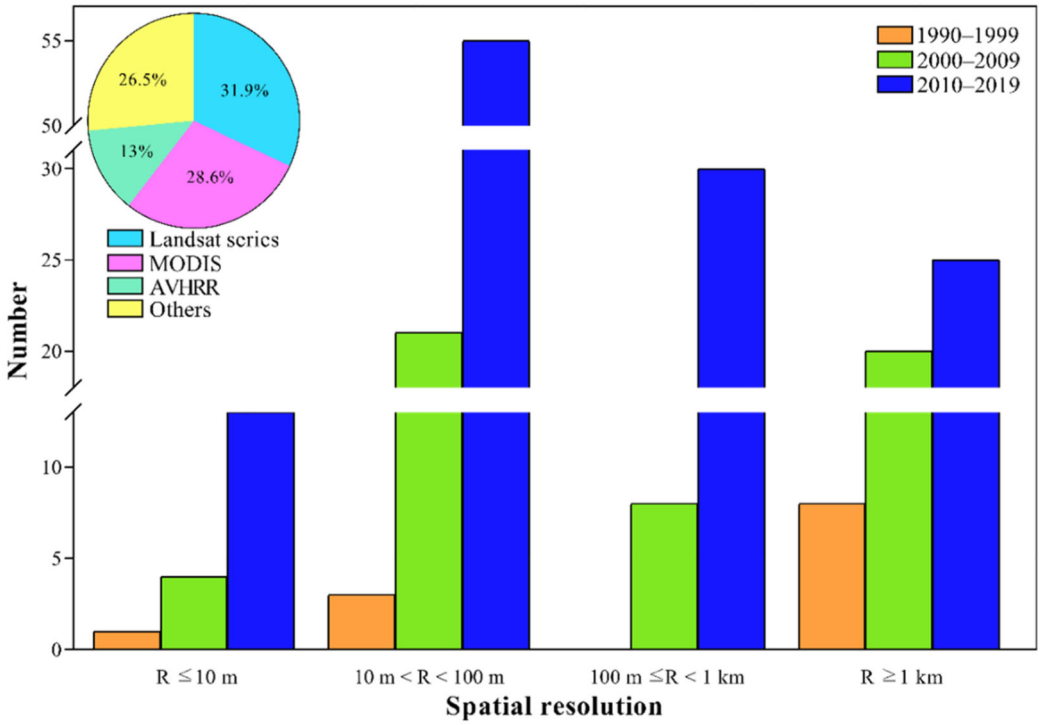


**Fig. 4. Number (*x*-axis) of RA algorithms applied to the remotely sensed data obtained from sensors or database (left *y*-axis) with various spatial resolutions (right *y*-axis) between 1990 and 2019.**




Europe PMC Funders Author Manuscripts

Europe PMC Funders Author Manuscripts

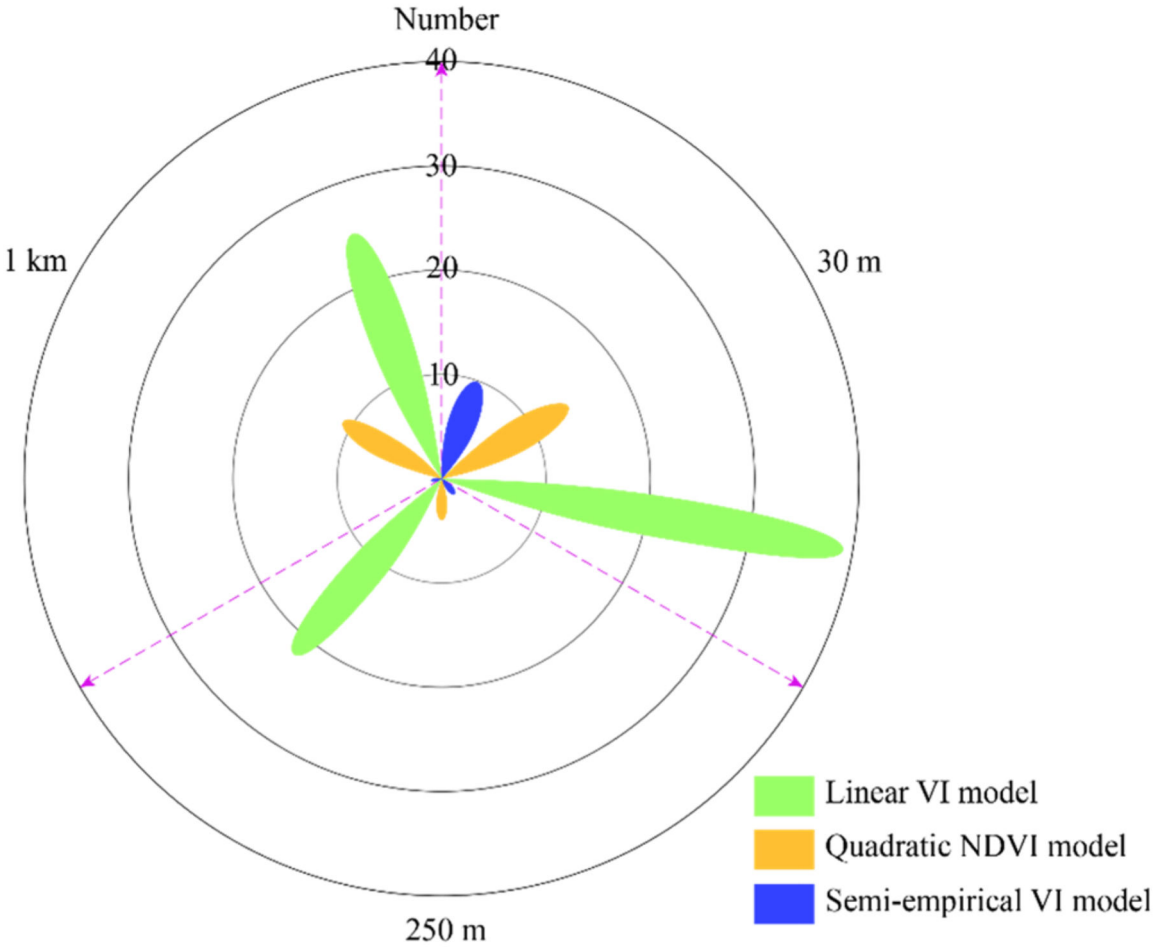


**Fig. 5. Number of RA algorithms (excluding the NDVI mixture model) applied to remotely sensed images with 30-m, 250-m, and 1-km spatial resolutions.**

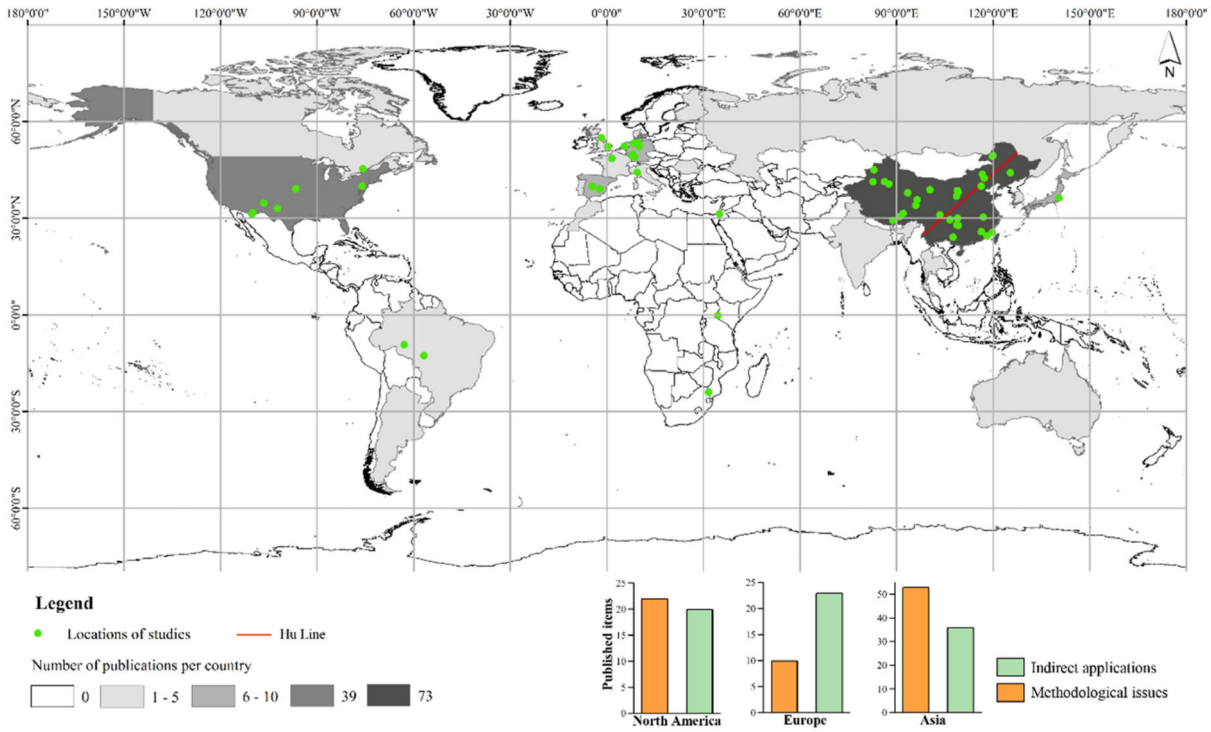


**Fig. 6. World map displaying the geographic distribution of the selected studies.**




Europe PMC Funders Author Manuscripts

Europe PMC Funders Author Manuscripts



*ISPRS J Photogramm Remote Sens*. Author manuscript; available in PMC 2022 September 07.

**Table 1**

**Summary of techniques/algorithms of the considered approaches used to determine the ($NDVI_{\infty}$ and $NDVI_S$) thresholds.**

| Technique/algorithm | Case study | | | |
|---|---|---|---|---|
| | Reference | Main functional vegetation types | $NDVI_{\infty}$ | $NDVI_s$ |
| Identification of pure vegetation or bare soil pixel based on field measurements (e.g., GPS points, field-measured spectral data) or higher-resolution remotely sensed images | Wang and Qi (2008) | Forest | 0.71 | 0.16 |
| | Imukova et al. (2015) | Crop | 0.95 | 0.05 |
| | Jiao et al. (2014) | Forest and shrubbery | 0.78 | 0.03 |
| Analysis of remotely sensed images to obtain the accumulative maximum and minimum NDVI values (within a long-term series for a predefined land category classified by classifiers) in the investigated area | Ge et al. (2008) | Forest, crop, grassland, shrubbery | 0.86 | 0.05 |
| | Wang et al. (2014) | Forest, crop | 0.65 | 0.05 |
| Application of end-member extraction approaches (e.g., the PPI method or two-dimensional feature space plots) to determine minimum and maximum values | Jia et al. (2017) | Crop | 0.941 | 0.068 |
| Inversion of the relationship between the remotely-derived NDVI and the actual fractional vegetation cover | Xiao and Moody (2005) | Grassland, shrubbery, woodland | 0.637 | −0.054 |
| | Kuang et al. (2015) | Crop, forest, grassland | 0.59 | 0.04 |
| Theoretically fixed values from the radiative transfer model | Liu et al. (2008) | Crop | 0.935 | 0.121 |
| Adaptation of the frequency histogram of the periodical maximum NDVI values (for each pixel for each biome classified by the auxiliary data, e.g., the land cover category and soil database) or cumulative percentages of NDVI in the entire study area based on image statistics | Zeng et al. (2000); Miller et al. (2006) | Forest, grassland, crop | 75th percentile of the annual maximum NDVI | 0.05 by the 5th percentile of the annual maximum NDVI for barren |
| | | Shrubbery | 90th percentile of the annual maximum NDVI | |
| | Verger et al. (2009) | Crop | 0.87 | 0.18 |
| | Li et al. (2005) | Crop | 0.89 | 0.1 |
| | Ge et al. (2018) | Grassland | 99.5% cumulative percentage of the NDVI | 0.5% cumulative percentage of the NDVI |
| Adoption of spatial interpolation technologies | Johnson et al. (2012) | Forest | – | – |
| Use of *in situ* measurements with a substantial spectral signal gap between *in situ* measurement and the pure pixel endmember value | Li et al. (2014) | Grassland | *In situ:* 0.891 | 0.203 |
| | | | MODIS: 0.806 | 0.118 |
| | | | Landsat-8 OLI: 0.807 | 0.119 |
| Combination of multi-angle reflectance characteristics and the Beer-Lambert law | Song et al. (2017) | Crop | 0.903 | 0.072 |

Europe PMC Funders Author Manuscripts



| Technique/algorithm | Case study | | | |
|---|---|---|---|---|
| | Reference | Main functional vegetation types | $NDVI_{\infty}$ | $NDVI_s$ |
| | | Grassland/Forest | 0.908 | 0.029 |
| | Mu et al. (2018) | Crop, grassland, forest, shrubbery | – | – |

Abbreviations: MODIS = Moderate Resolution Imaging Spectroradiometer; OLI = Operational Land Imager.

Europe PMC Funders Author Manuscripts

**Table 2**

Relevant journals that have published four or more of the papers related to RA algorithms. The search was conducted on November 5, 2019.

| Journals | Number of papers |
|---|---|
| Remote Sensing | 21 |
| Remote Sensing of Environment | 21 |
| International Journal of Remote Sensing | 19 |
| International Journal of Applied Earth Observation and Geoinformation | 7 |
| IEEE Transactions on Geoscience and Remote Sensing | 6 |
| Agricultural and Forest Meteorology | 4 |
| ISPRS Journal of Photogrammetry and Remote Sensing | 4 |
| Hydrology and Earth System Sciences | 4 |